Mechanism of voltage-sensitive fluorescence in a microbial rhodopsin

Dougal Maclaurin[a,1], Veena Venkatachalam[b,1], Hohjai Lee[c], and Adam E. Cohen[a,c,2]

[a]Department of Physics, [b]Graduate Program in Biophysics, and [c]Department of Chemistry and Chemical Biology, Harvard University, Cambridge, MA 02138

Edited by Steven G. Boxer, Stanford University, Stanford, CA, and approved March 4, 2013 (received for review September 12, 2012)

Microbial rhodopsins were recently introduced as genetically encoded fluorescent indicators of membrane voltage. An understanding of the mechanism underlying this function would aid in the design of improved voltage indicators. We asked, what states can the protein adopt, and which states are fluorescent? How does membrane voltage affect the photostationary distribution of states? Here, we present a detailed spectroscopic characterization of Archaerhodopsin 3 (Arch). We performed fluorescence spectroscopy on Arch and its photogenerated intermediates in *Escherichia coli* and in single HEK293 cells under voltage-clamp conditions. These experiments probed the effects of time-dependent illumination and membrane voltage on absorption, fluorescence, membrane current, and membrane capacitance. The fluorescence of Arch arises through a sequential three-photon process. Membrane voltage modulates protonation of the Schiff base in a 13-*cis* photocycle intermediate ($M \rightleftharpoons N$ equilibrium), not in the ground state as previously hypothesized. We present experimental protocols for optimized voltage imaging with Arch, and we discuss strategies for engineering improved rhodopsin-based voltage indicators.

Optical recording of membrane potential promises new insights into the individual and collective dynamics of neurons (1, 2), cardiac cells (3), developing embryos (4), and even microbes (5). Despite decades of effort (2, 6, 7), development of effective voltage indicators remains a challenge. We recently discovered that the endogenous fluorescence of some microbial rhodopsin proteins responds sensitively and quickly to changes in membrane voltage (8, 9). Heterologous expression of Archaerhodopsin 3 (Arch) in cultured neurons enabled robust optical recordings of action potentials using a genetically encoded indicator. However, the mechanisms by which these proteins fluoresced and sensed voltage remained obscure. A detailed photophysical understanding of GFP proved essential to its optimization and diversification (10). Thus, we adopted a similar approach for Arch. The aims of this paper are (*i*) to identify optimal imaging conditions for Arch and (*ii*) to explain how Arch functions as a voltage indicator.

Arch (Uniprot P96787) is a microbial rhodopsin derived from the Dead Sea microorganism *Halorubrum sodomense*. The protein contains seven transmembrane α-helices with the chromophore retinal covalently bound via a Schiff base to a lysine in the protein core. In the wild, Arch serves as a light-driven outward proton pump, capturing solar energy for its host (11). Upon expression in neurons, Arch can act as an optogenetic neural silencer: illumination with green light generates a hyperpolarizing photocurrent, which suppresses neural firing (12).

Illumination with orange or red light excites Arch fluorescence; emission is in the near infrared, peaked at 710 nm (8). Fluorescence is sensitive to membrane voltage; with excitation at 640 nm, fluorescence increased twofold from −150 to +150 mV, with a response time of ∼0.6 ms. However, Arch has two undesirable attributes as a voltage indicator. First, the fluorescence is very dim, requiring intense laser illumination to be detectable. Second, illumination of Arch slightly perturbs the membrane potential: under typical illumination for imaging (640 nm, 230 W/cm^2), Arch generates an outward photocurrent in neurons of 34 ± 7 pA ($n = 7$ cells), which hyperpolarizes the membrane by 6.2 ± 1.1 mV. A mechanistic understanding of Arch could guide efforts to engineer improved performance.

The photocycle of Arch is likely similar to that of its close homolog bacteriorhodopsin (BR) (*SI Appendix*, Fig. S1), which we take as a template. Light-induced isomerization of retinal in BR induces a series of conformational shifts that moves one proton across the membrane. In the ground state (g), the retinal is in an *all-trans* conformation and the Schiff base is protonated. Absorption of a green or yellow photon induces photoisomerization to a 13-*cis* conformation ($g \rightarrow L$), followed by proton transfer from the Schiff base to an acceptor on the extracellular side ($L \rightarrow M_1$). The Schiff base then switches accessibility to the cytoplasmic side ($M_1 \rightarrow M_2$), where a proton donor reprotonates the Schiff base ($M_2 \rightarrow N$). The donor takes up a proton from the cytoplasm and the retinal thermally isomerizes back to *all-trans* ($N \rightarrow O$). Finally, the acceptor releases its proton to the proton-release complex on the extracellular side ($O \rightarrow g$). All photocycle intermediates except for M have overlapping absorption spectra peaked between 550 and 630 nm; due to the deprotonated Schiff base, the M intermediates absorb maximally at 410 nm. Although the photocycle was initially viewed as a series of sequential steps (13, 14), kinetic evidence suggests rapid equilibrium among the states within the 13-*cis* manifold (15–17). Excitation of photocycle intermediates generates off-pathway states, some of which have been reported to be fluorescent (18–21).

We previously speculated that voltage acted by modifying the protonation of the Schiff base in the ground state of Arch. However, illumination at 230 W/cm^2, typical for imaging, corresponds to $>10^4$ photon absorption events per molecule per second. Microbial rhodopsin photocycles typically last ∼10 ms. Thus, under photostationary imaging conditions, the ground state may be significantly depleted. Each photocycle intermediate has a different charge distribution, and thus the relative energy of intermediates depends on membrane voltage. A realistic model must acknowledge that fluorescence and voltage sensitivity could arise anywhere in the photocycle.

Early transient absorption measurements on BR in vesicles indicated that hyperpolarizing voltage slowed the decay of an M state (22–24). However, the membrane voltage was not precisely known in these experiments. Measurements of photocurrents in BR under patch-clamp conditions further indicated a voltage-dependent M-state decay (25–27). *Acetabularia* rhodopsin behaved similarly, but a differing kinetic model led to the conclusion that voltage primarily acted to slow the O-state decay (28).

Here, we combine patch-clamp measurements with fluorescence spectroscopy of Arch and its photogenerated intermediates (Fig. 1). In *Results*, *Optimization of Voltage Imaging*, we characterize the fluorescence, photocurrent, and voltage sensitivity spectra of Arch and the nonpumping mutant Arch(D95N) under steady-state illumination. This information enables straightforward optimization of imaging parameters and is intended for

Author contributions: D.M., V.V., H.L., and A.E.C. designed research; D.M., V.V., and H.L. performed research; D.M., V.V., and A.E.C. analyzed data; and D.M., V.V., and A.E.C. wrote the paper.

The authors declare no conflict of interest.

This article is a PNAS Direct Submission.

[1]D.M. and V.V. contributed equally to this work.

[2]To whom correspondence should be addressed. E-mail: cohen@chemistry.harvard.edu.

This article contains supporting information online at www.pnas.org/lookup/suppl/doi:10.1073/pnas.1215595110/-/DCSupplemental.

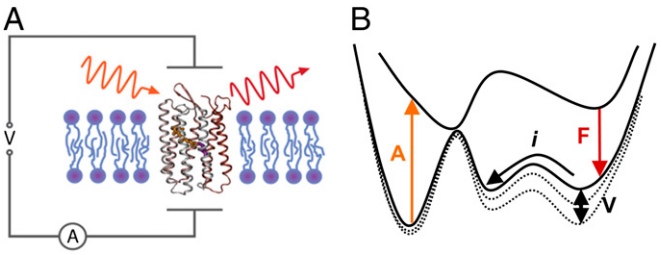

Fig. 1. Multimodal spectroscopy of a microbial rhodopsin. (*A*) Optical and electrical perturbations induce fluorescence and photocurrent responses. Rhodopsins have strong cross-modality couplings (illumination modulating current; voltage modulating fluorescence) as well as nonlinear optical and electrical responses. (*B*) Dynamics on a potential energy landscape. Absorption (A), fluorescence (F), and photocurrent (*i*) probe distinct types of transitions, whereas voltage modulates the shape of the landscape.

readers wishing to perform voltage-imaging experiments. In *Results*, *Photocycle of Arch*, we study the transient absorption and transient fluorescence of Arch to characterize the photocycle. In *Results*, *Optoelectronic Properties of Arch*, we combine optical with electrical measurements to probe cross-couplings between illumination and current, and between voltage and fluorescence. We conclude that fluorescence arises through a sequential three-photon process and that membrane voltage tips the relative balance of an *M*-like and an *N*-like intermediate.

Results

Optimization of Voltage Imaging. We sought to determine the illumination conditions (wavelength and intensity) most conducive to voltage imaging and least perturbative to membrane potential. The apparatus consisted of an inverted epifluorescence microscope equipped with multiple laser lines, combined with a patch-clamp electrophysiology rig (*SI Appendix*, Fig. S2). We expressed Arch in HEK293T cells and recorded fluorescence and photocurrent as a function of illumination wavelength, illumination intensity, and membrane voltage. All experiments were performed at 25 °C unless otherwise indicated.

Under steady-state high-intensity illumination (1,000 W/cm^2, 594 nm), Arch fluorescence increased by $\Delta F/F = 35\%$ between −150 and +150 mV [under 640-nm illumination, the sensitivity was $\Delta F/F = 100\%$ for the same voltage range (8)]. A fit to a Hill curve showed that the voltage-sensitive transition experienced a fraction $\alpha \sim 0.15$ of the total membrane voltage (*SI Appendix*). We used a photomultiplier to measure the fluorescence response to a step in applied voltage (Fig. 2*B*, and *SI Appendix*, Fig. S3). The membrane voltage lagged the applied voltage by ∼0.4 ms due to the *RC* charging time of the membrane. After accounting for this lag analytically, we found that the protein step response had a time constant of 0.6 ms (*SI Appendix*).

A puzzle in our initial experiments was the relative ease with which we imaged Arch in the microscope, compared with the reported extremely low fluorescence quantum yield (10^{-4}–10^{-3}) of all known microbial rhodopsins (20, 29, 30). The fluorescence of BR was reported to increase faster than linearly with increasing excitation intensity (31). We thus measured Arch fluorescence, *F*, as a function of illumination intensity, *I* [excitation (exc.), 532, 594, or 640 nm; emission (em.), 660–760 nm] in a sample of fractionated *Escherichia coli* membranes containing an Arch-eGFP fusion (Fig. 2*C*). Indeed, the relative brightness of Arch (*F*/*I*) increased at higher illumination intensity, growing 10-fold between 0.05 and 200 W/cm^2 (exc., 594 nm). In contrast, eGFP showed *F*/*I* independent of illumination intensity (exc., 488 nm; em., 511–551 nm). We previously reported that under dim illumination Arch was 500-fold dimmer than eGFP (8). Our present results show that, under intense illumination, Arch is only 50-fold dimmer than eGFP. We measured the photocurrent as a function of illumination intensity and observed saturation behavior: under intense illumination, additional light did not lead to additional photocurrent (*SI Appendix*, Fig. S4).

We visually demonstrated the nonlinear increase in Arch fluorescence with increasing illumination intensity in a cuvette of purified Arch-eGFP fusion protein. The cuvette was illuminated with focused continuous-wave (CW) illumination at 473 nm (2 μW, to excite eGFP) and 594 nm (5 μW, to excite Arch) (Fig. 2*D* and *SI Appendix*). Although eGFP fluoresced throughout the beam path, Arch fluoresced predominantly at the focus. This nonlinear increase in Arch fluorescence occurred at an intensity ∼10^{10}-fold lower than typically required for two-photon microscopy, implying a sequential multiphoton process in Arch, in contrast to the coherent multiphoton excitation commonly observed with pulsed femtosecond excitation.

We measured four key action spectra of Arch: photocurrent, ground-state absorbance, fluorescence excitation, and voltage sensitivity of fluorescence (*SI Appendix*). Due to the nonlinear dependence of Arch fluorescence on illumination intensity, we took care to maintain constant illumination intensity of 10 W/cm^2 across all wavelengths. Arch generated the largest photocurrent when excited at 530 nm (typically ∼40 pA), absorbed maximally at 552 nm (extinction coefficient 50,300 $M^{-1}\cdot cm^{-1}$; *SI Appendix*, Fig. S5), showed maximal fluorescence (*F*) when excited at 570 nm and exhibited maximal change in fluorescence (ΔF) upon a voltage step when excited at 590 nm. Due to the differing spectra of *F* and ΔF, the peak in the fractional voltage sensitivity, $\Delta F/F$, occurred at a different wavelength (640 nm; *SI Appendix*, Fig. S6*A*) than the peak in ΔF (590 nm; Fig. 2*E*). These differing spectra further indicate that optical excitation of multiple states is involved in determining the photoresponse of Arch.

These findings inform the choice of optics used to image Arch. To maximize voltage sensitivity and to minimize photocurrent, the illumination should be red or orange. Although green illumination produces comparatively strong fluorescence, this fluorescence is not sensitive to voltage. With conventional fluorophores one can trade exposure time for illumination intensity to maintain a constant signal. Due to the multiphoton excitation of Arch, this tradeoff is not possible. Illumination with a light-emitting diode or arc lamp produces barely detectable fluorescence, whereas intense illumination (typically from a laser) leads to a robust signal.

We previously introduced the mutant Arch(D95N) as a nonpumping voltage reporter. We characterized Arch(D95N) by the same measures as in Fig. 2 (*SI Appendix*, Fig. S7). This mutant had a slower response time than wild-type Arch, with a minor (∼20%) component occurring in <1 ms, and a major (∼80%) component lasting 36 ms rising, 30 ms falling at 25 °C. Remarkably, at 35 °C the fast component grew significantly, accounting for ∼55% of the response. These results will be useful to researchers interested in using Arch(D95N) as a voltage indicator. The fractional voltage sensitivity of wild-type Arch, $\Delta F/F$, was relatively insensitive to illumination intensity between 10 and 1,000 W/cm^2, whereas for Arch(D95N) $\Delta F/F$ increased threefold to fivefold over this range, depending on the excitation wavelength (*SI Appendix*, Fig. S6).

Photocycle of Arch. Transient absorption spectra of detergent-solubilized Arch were recorded with excitation by a nanosecond pulsed Nd:YAG laser at 532 nm (Fig. 3 *A* and *B*). These spectra closely matched corresponding spectra of Archaerhodopsin 1 (32) and BR (33). The pH-dependent transient absorption (Fig. 4*C*, below) suggested a slowing of *M* formation at pH 6, consistent with proton release preceding *M* formation. Formation of *O* was slower at pH 8, indicating that proton uptake preceded *O* formation. As with BR, Arch showed dark adaptation. When left in the dark for several minutes, Arch spontaneously converted into a state with increased initial fluorescence upon onset of illumination (*SI Appendix*, Fig. S8). In BR, dark adaptation corresponds to conversion from *all-trans* retinal to a mixture of *all-trans* and 13-*cis* retinal (34).

The ambiguities in inferring a kinetic model from transient absorption alone have been well documented (33, 35). Based on the strong sequence and spectroscopic homology between Arch and

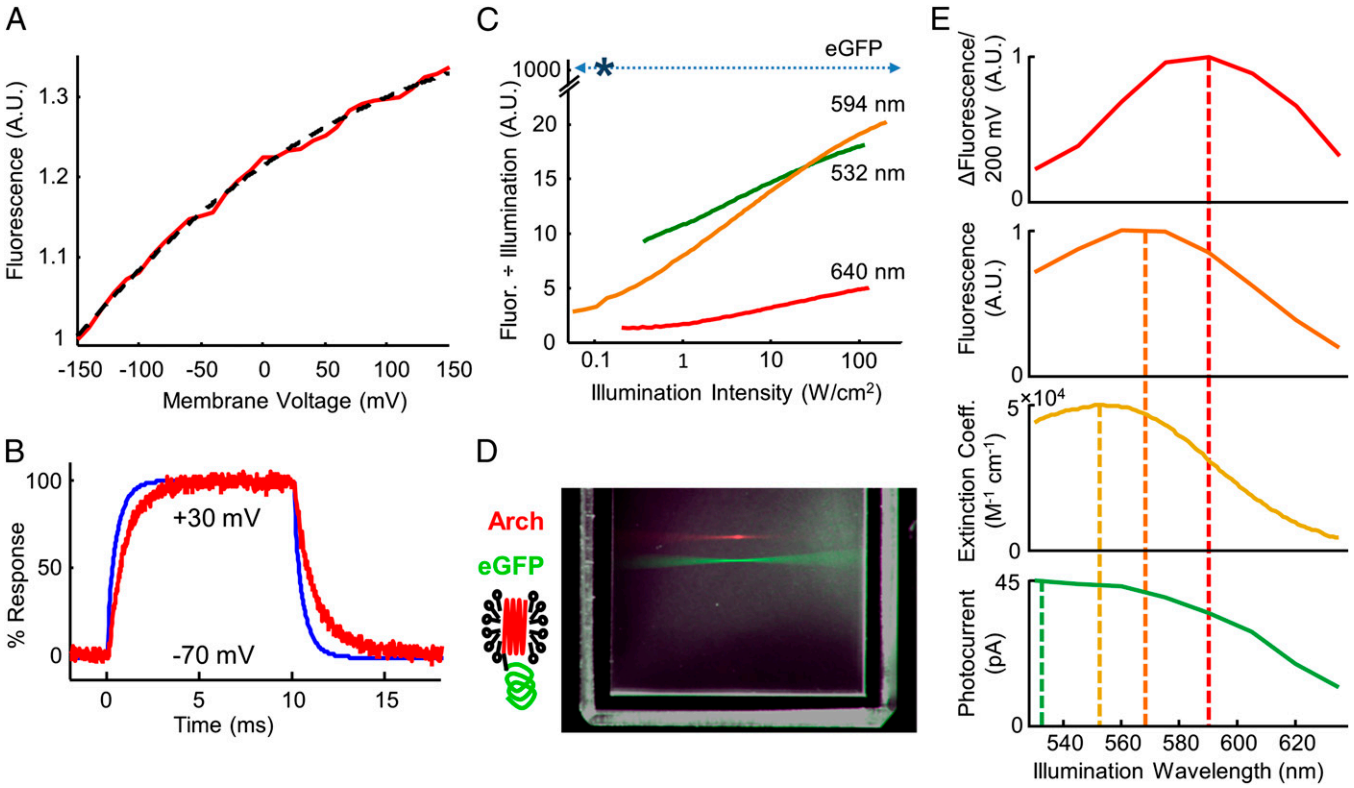

Fig. 2. Arch as a voltage indicator. (*A*) Voltage-sensitive fluorescence of Arch (exc., 594 nm; 1,000 W/cm^2; em., 660–760 nm). The dashed line is a fit to a two-state Boltzmann distribution (*SI Appendix*). (*B*) Fluorescence response (red) to a voltage step from −70 to +30 mV (blue). The time constant of the voltage step arose from capacitive charging of the membrane (*SI Appendix*). (*C*) Ratio of fluorescence to illumination intensity (*F/I*), as a function of illumination intensity. (*D*) Visual demonstration of nonlinear dependence of Arch fluorescence on CW illumination intensity. Two laser beams were focused inside a cuvette containing an Arch-eGFP fusion. The top beam (594 nm) excited fluorescence from Arch. The identically shaped bottom beam (473 nm) excited fluorescence from eGFP. Arch fluorescence was localized to the focus, whereas eGFP fluorescence occurred throughout the beam. Image is a pseudocolored composite of three exposures taken under different camera settings (*SI Appendix*). (*E*) Action spectra of Arch showing distinct spectra for different quantities.

BR, we assumed a BR-like photocycle and used the transient absorption data to infer rate constants. Fig. 3*B* shows the fit of this model to some of the transient absorption data. This model indicates that a blue-absorbing *M* state formed within 50 μs and decayed with a time constant of 390 μs. A red-absorbing *O* state arose with two time constants of 390 μs and 4.1 ms, and decayed with a time constant of 14 ms. The *N* state is not directly visible in the transient absorption due to its strong spectral overlap with the ground state. Fitting parameters are given in *SI Appendix*, Table S1.

To determine which intermediate state (or states) produced fluorescence, we performed transient fluorescence experiments on fractionated *E. coli* membranes containing Arch. An intense green pump pulse (50 W/cm^2, 100 μs, 532 nm) initiated the photocycle. A weak red probe pulse (15 W/cm^2, 100 μs, 640 nm) excited fluorescence with variable delay after the pump.

Illumination with the probe alone produced barely detectable fluorescence [Fig. 3*C*, (i)], consistent with the expected low fluorescence quantum yield of the Arch ground state. Application of a single pump pulse before the probe produced a species more than twice as fluorescent as the ground state. This species appeared in <20 μs and decayed with a time constant of 1.0 ms [Fig. 3*C*, (ii)]. Remarkably, application of two pump pulses before the probe [timing shown in Fig. 3*C*, (iii)] produced up to sixfold more fluorescence than the ground state. Fluorescence peaked with an interval of 10 ms between the pump pulses [Fig. 3*C*, (iii)]. These experiments established that the fluorescence of Arch arises from a sequential three-photon process: one photon to initiate the photocycle, a second to generate the fluorescent species from a photointermediate, and a third photon to induce fluorescence.

We characterized the action spectra and saturation properties of each of the three photons (*SI Appendix*, Figs. S9–S11). Photon 1 matched the ground-state absorption spectrum of Arch. Photon 2 was blue-shifted by 10 nm relative to photon 1. In BR, the *N* state has a 10-nm blue shift relative to the ground state, so we provisionally assign photon 2 to excitation of an *N*-like intermediate. Photon 3 peaked at 570 nm. At low intensities of pumps 1 and 2, the fluorescence from pump 3 was linear in all three pump intensities, confirming that each contributed a single photon. We also measured the spontaneous decay (presumably back to *N*) of the fluorescent state, and found a time constant of 0.84 ms. We combined the transient absorption and fluorescence data to propose a photocycle shown in Fig. 3*D*.

Ohtani and coworkers (20, 31, 36) found that in BR sequential absorption of two photons generated a state, termed *Q*, which could be excited by a third photon to yield fluorescence. [The term "*Q*" state has been used to represent other intermediates in the BR photocycle (18). Here, we refer exclusively to the Ohtani *Q*.] This state had an excited state lifetime of 62 ps, vs. ∼500 fs for the ground state, and was thus ∼100-fold more fluorescent than the ground state (36). The *Q* state was excited by red light and emitted in the near infrared with a peak at ∼720 nm. The timing in the photocycle, excitation and emission spectra, and thermal relaxation rate of our fluorescent state match the Ohtani *Q* state, so we designate the dominant fluorescent state *Q*.

The complex photophysics of Arch fluorescence have important implications for its use as a fluorescent label in confocal microscopy. During a frame-scanning confocal measurement, each molecule experiences microsecond bursts of intense illumination, spaced by hundreds of milliseconds of darkness. These bursts are shorter than the time required for Arch to enter the

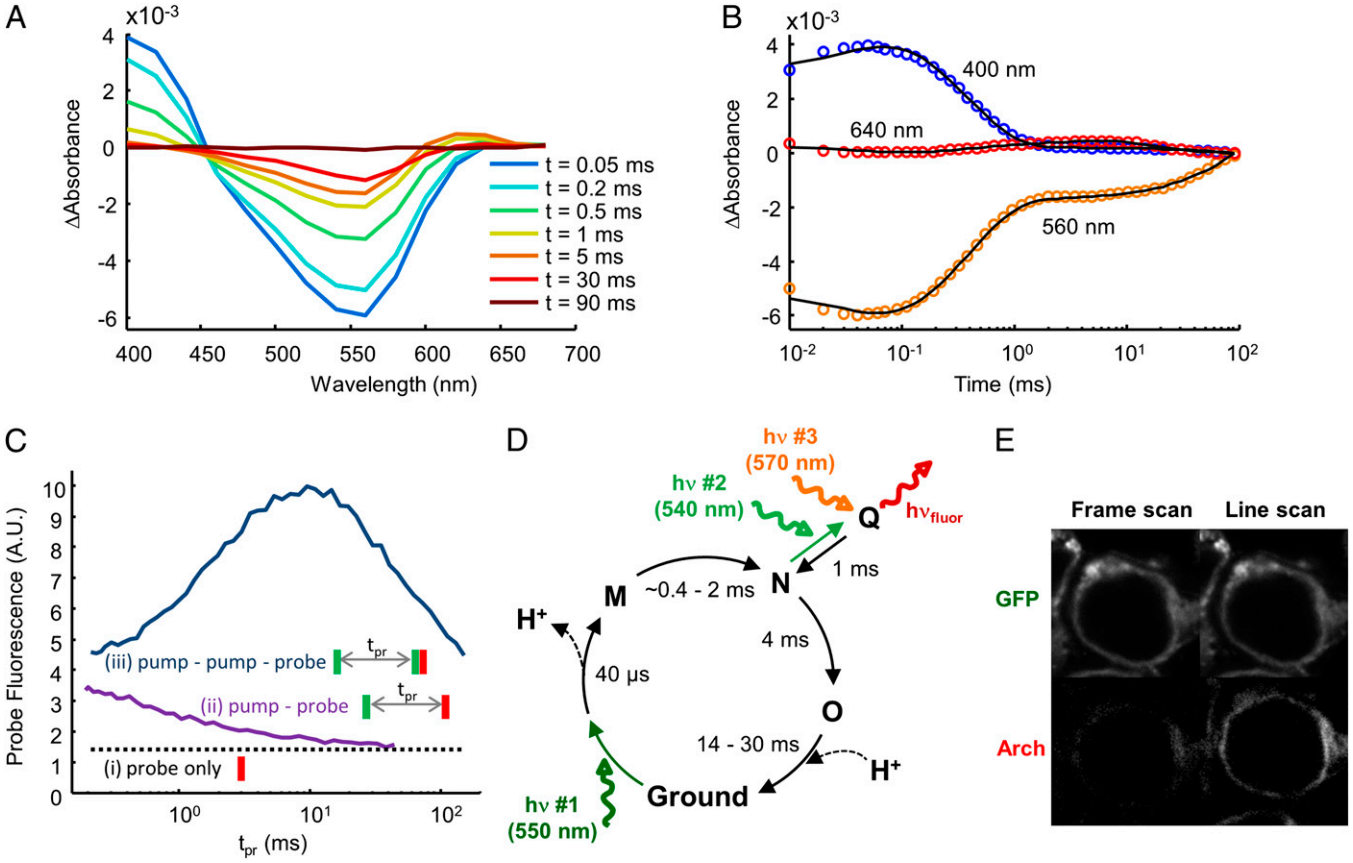

Fig. 3. Time-resolved spectroscopy of Arch. (*A*) Transient absorption spectra showing early rise of a blue-shifted *M* intermediate, and late rise of a red-shifted *O* intermediate. (*B*) Time-dependent absorption data are well described by a fit to four exponential decays. (*C*) Transient fluorescence experiments established that fluorescence was dominated by a sequential three-photon process. (*D*) Proposed photocycle with rates derived from transient absorption and transient fluorescence data. (*E*) Confocal scans showing the effects of scan speed on brightness. Arch fluorescence was sensitive to the timing of the illumination, whereas eGFP fluorescence was not.

fluorescent Q state, and the interburst interval is longer than the photocycle. Thus, under frame-scanning conditions, Arch appeared very dim (Fig. 3*E*). In line-scanning mode, each line of the image was scanned multiple times before the laser advanced to the next line. The interval between line scans (~0.5 ms) was shorter than the photocycle, so the illumination in each scan sensitized fluorescence in subsequent scans. Arch then appeared brighter. In an Arch-eGFP fusion, the brightness of eGFP was independent of the scan mode.

Optoelectronic Properties of Arch. To identify states whose population depended on voltage, we transiently expressed Arch in HEK293T cells, and recorded membrane current $i(t)$ and fluorescence $F(t)$ as functions of the membrane voltage $V_m(t)$ and illumination $I(\lambda,t)$. Three attributes of voltage-sensitive fluorescence were immediately striking: (*i*) A step in illumination (from darkness) under constant voltage induced fluorescence that was initially not sensitive to membrane voltage (Fig. 4*A*). Fluorescence became sensitive to voltage with a time constant of 2 ms. (*ii*) A step in voltage under constant illumination induced a fluorescence response with a time constant of 0.6 ms (Fig. 2*A*). (*iii*) An initial flash of light sensitized the protein so that fluorescence from a second flash was (*a*) brighter than fluorescence from an isolated flash, and (*b*) sensitive to voltage (Fig. 4*B*). Both forms of sensitization arose with a time constant of 2 ms and fell with a time constant of 30 ms.

Observation (*i*) rules out a voltage-dependent change in the ground state as the origin of voltage-dependent fluorescence, in contrast to our previously proposed model (8). Observation (*ii*) requires that the voltage-sensitive step be fast, and either involve the fluorescent state directly, or be coupled to the fluorescent state by fast rate constants. Observation (*iii*) establishes that the voltage-sensitive manifold is long lasting. Thus, the fast voltage-sensitive rate is preceded by a somewhat slower step and is followed by a much slower step in the photocycle.

Two other measurements pointed to a long-lived voltage-sensitive intermediate. In a double-flash experiment, the photocurrent from the second flash was smaller than from the first, recovering with a time constant of 32 ms (a two-exponential fit yielded time constants of 3.8 and 54 ms; *SI Appendix*, Fig. S12). The photocurrent recovery reflects ground-state repopulation and thus indicates a long-lived intermediate.

We performed an electrical test for a voltage-dependent equilibrium in this long-lived intermediate by measuring membrane capacitance as a function of time after a single flash (*SI Appendix*, Fig. S14). A voltage-dependent chemical equilibrium must increase membrane capacitance through the voltage-dependent charge redistribution. We observed a flash-induced increase in membrane capacitance that recovered on a 30-ms timescale (Fig. 4*B*). The maximum light-induced change in capacitance was $\delta C = 0.1$ pF, on a baseline membrane capacitance of $C = 41$ pF. Although the transient capacitance provides mechanistic insight, its magnitude $\delta C/C = 0.25\%$ suggests that light-induced capacitive loading is negligible.

By fitting the amplitude of the transient capacitance to a two-state model at thermal equilibrium (*SI Appendix*), we inferred that the relative energies of the two states in voltage-dependent equilibrium were shifted by an energy αV_m, with $\alpha = 0.1$. This value is in reasonable agreement with the value $\alpha = 0.15$ extracted from a fit of a Hill curve to the plot of F vs. V_m (Fig. 2*A*).

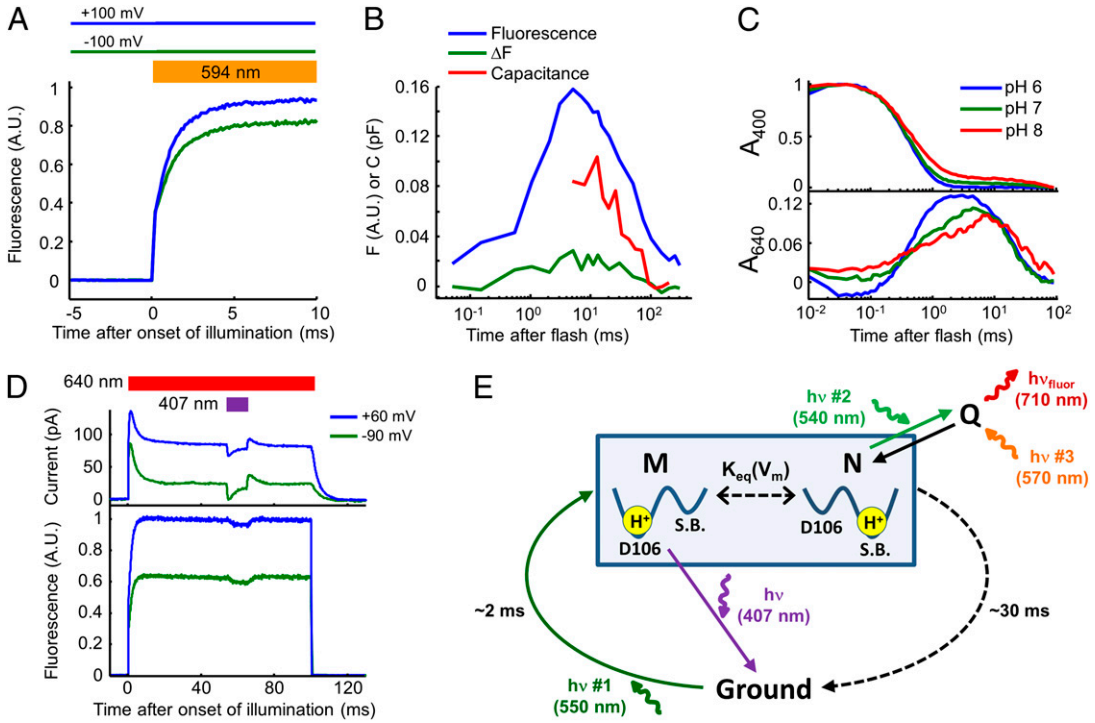

Fig. 4. Optoelectronic dynamics of Arch. (*A*) Fluorescence response of Arch to a step in illumination at V_m = +100 and −100 mV. (*B*) Transient responses of Arch in a double-flash experiment. Fluorescence from the second flash rose and fell following initiation of the photocycle. The difference in fluorescence between +30 and −70 mV, Δ*F*, rose and fell with the fluorescence. A single flash induced a similar trajectory of membrane capacitance. (*C*) Transient absorption in solubilized Arch as a function of pH, normalized to the maximum signal at 400 nm. (*D*) Photocurrent and fluorescence in response to illumination with a pulse of red light, with a superimposed pulse of violet light. (*E*) A simplified model of voltage sensitivity and fluorescence in Arch. Photon #1 initiates the photocycle. Voltage modulates a proton-transfer equilibrium between two photocycle intermediates: an *M* state with a protonated donor (D106) and an *N* state with a protonated Schiff base (S.B.). Fluorescence arises through conversion of *N* to *Q* (photon #2) followed by electronic excitation of *Q* (photon #3).

The local access model of the BR photocycle proposes that all 13-*cis* photointermediates—*L*, M_1, M_2, and *N*—are in rapid equilibrium (16). Fluorescence arises from a branch off *N*, so we hypothesized that voltage acted within the 13-*cis* manifold. We further hypothesized that voltage acted by modulating the protonation of a fluorescence-determining functional group within the 13-*cis* manifold. Thus, a state whose population showed pH sensitivity near neutral pH would be a plausible voltage-sensitive state. We performed transient absorption spectroscopy on detergent-solubilized Arch as a function of pH. At pH 8, a long-lived *M* state appeared (Fig. 4*C*).

Based on the pH-dependent transient absorption, and the extensive literature suggesting a voltage-dependent *M* decay in BR, we tested whether membrane voltage tuned an $M \rightleftharpoons N$ equilibrium in Arch. This hypothesis was attractive because (*a*) an *M* state would not be excited by the red or orange laser, and thus could be a dark equilibrium partner with the prefluorescent *N* state; and (*b*) in the $M \rightarrow N$ transition, the Schiff base is reprotonated from the proton donor (D106), which resides between the Schiff base and the cytoplasm. The long range (10.5 Å in BR) and orientation of this proton-transfer would favor the nonfluorescent *M* state at negative voltage and the prefluorescent *N* state at positive voltage, consistent with the observed dependence of fluorescence on voltage.

To test this hypothesis, we used flashes of violet light (407 nm) to depopulate the *M* state under photostationary red light illumination. Violet light is known to induce 13-*cis* to *all-trans* isomerization in the *M* state, short-circuiting the photocycle from *M* to ground. Similar illumination protocols have been used in BR (25, 26) and in *Acetablularia* rhodopsin (28). We recorded the photocurrent and fluorescence under red and (red plus violet) illumination, as a function of membrane voltage.

Under photostationary red illumination, addition of violet light decreased the photocurrent and the fluorescence, indicating the presence of an *M*-state population (Fig. 4*D*). To test whether these data were consistent with a voltage-dependent $M \rightleftharpoons N$ equilibrium, we constructed a highly simplified model of the photocycle shown in Fig. 4*E*. The $M \rightleftharpoons N$ interconversion was assumed to be fast compared with the other rates, and thus always at equilibrium. Red illumination delivered population into the 13-*cis* manifold, while molecules relaxed back to ground at a rate proportional to the *N* population. Violet illumination introduced an additional relaxation pathway, with a rate proportional to the *M* population.

This model quantitatively reproduced (*a*) the shapes of the photocurrent and fluorescence transients upon onset of red illumination; (*b*) the dependence of steady-state fluorescence and photocurrent on membrane voltage under red illumination only; and (*c*) the effect of violet illumination on fluorescence and photocurrent (*SI Appendix*, Fig. S13). We thus conclude that a voltage-dependent $M \rightleftharpoons N$ equilibrium is a likely explanation for voltage-dependent fluorescence in Arch.

Due to the small number of states, the model could not reproduce the complex kinetics of ground-state recovery. This model does not rule out more complex mechanisms of voltage sensitivity, such as voltage-dependent equilibria among *L*, M_1, and M_2, or multiple voltage-dependent rates. Our data do not distinguish between these scenarios.

Discussion

The ground state of Arch is only weakly fluorescent, but a photogenerated intermediate is roughly 10-fold brighter than previously thought. Fluorescence arises through sequential action of three photons. Voltage sensitivity is a property of a 13-*cis* photocycle intermediate, not the ground state, and likely arises

through protonation of the Schiff base from the cytoplasmic side (i.e., a voltage-dependent $M \rightleftharpoons N$ equilibrium). The free energy of this reaction has a component equal to αV_m, with $\alpha \sim 0.15$; or in the language of electrophysiology, the gating charge is ~0.15 e. Many fluorescent voltage indicators significantly increase membrane capacitance, leading to electrical loading of the cell. Arch only acts as a voltage sensor in a photocycle intermediate, and in this intermediate the fractional increase in membrane capacitance is $\delta C/C < 1\%$.

A clear strategy for increasing the voltage sensitivity and brightness of Arch is to generate a protein with a 13-*cis* ground state or a metastable 13-*cis* intermediate. For instance, the D96N and D96N/D115N mutations of BR are known to prolong the lifetime in the 13-*cis* manifold (37), so homologous mutations in Arch (D106N, D125N) may enable voltage imaging under lower illumination intensities.

We further propose that mutations on the extracellular side designed to block current (such as D95N in Arch) are more likely to preserve voltage sensitivity than are mutations on the cytoplasmic side. The fluorescent *Q* state is reached by photoexcitation of the 13-*cis N* state. Thus, *Q* is unlikely to be exclusively 13-*cis*, but its isomerization state is not known. A structural model of *Q* would facilitate efforts to engineer proteins with improved brightness.

The differing spectra of *F* and ΔF (Fig. 2*E*), and the presence of fluorescence immediately upon illumination (Figs. 3*C* and 4*A*) indicate that the photocycle may contain two (or more) fluorescent species, not all of which are voltage sensitive. Our study has focused on the dominant voltage-sensitive species. The other fluorescent state(s) await characterization. Furthermore, under simultaneous illumination at two wavelengths within the visible (530–640 nm) the fluorescence and photocurrent depended in a complex way on the wavelengths and relative intensities of the illumination (*SI Appendix*, Fig. S15). These effects likely arise from additional light-driven pathways not included in our simple models.

The rich spectroscopic and optoelectronic properties of microbial rhodopsins have previously been considered for application in optical information processing and data storage (38). Although such applications have not yet been widely adopted, the ability of rhodopsins to transduce light into changes in membrane voltage have enabled many optogenetic tools. We propose that optoelectronic coupling in the opposite direction—changes in membrane voltage affecting optical properties—will enable a similarly broad set of applications in bioimaging.

Materials and Methods

Transient absorption experiments were performed on purified protein in a homemade transient absorption spectrometer. All other experiments were performed on a homemade inverted fluorescence microscope, equipped with time-gated illumination at multiple wavelengths, time-resolved detection, and a patch-clamp electrophysiology rig. HEK293T cells were grown following standard protocols and transiently transfected with the gene of interest. Cells were subjected to time-varying illumination and time-varying membrane voltage, and the ensuing fluorescence and membrane current were digitized and recorded. Details are provided in *SI Appendix*.

ACKNOWLEDGMENTS. We thank Joel Kralj, Daniel Hochbaum, Jeehae Park, and Lucy Rosenbaum for discussions and assistance with tissue culture. This work was supported by Presidential Early Career Award for Scientists and Engineers Award N00014-11-1-0549, the Harvard Center for Brain Science, National Institutes of Health (NIH) Grants 1-R01-EB012498-01 and New Innovator Grant 1-DP2-OD007428, the Harvard/Massachusetts Institute of Technology Joint Research Grants Program in Basic Neuroscience, a Herchel Smith Graduate Fellowship (to V.V.), NIH Medical Scientist Training Program Grant T32GM07753-33 (to V.V.), and a Frank Knox Memorial Fellowship (to D.M.).

1. Scanziani M, Häusser M (2009) Electrophysiology in the age of light. *Nature* 461(7266):930–939.
2. Peterka DS, Takahashi H, Yuste R (2011) Imaging voltage in neurons. *Neuron* 69(1):9–21.
3. Kaestner L, Tian Q, Lipp P (2012) Action potentials in heart cells. *Fluorescent Proteins II*, ed Jung G (Springer, Berlin), pp 163–182.
4. Adams DS, Masi A, Levin M (2007) H^+ pump-dependent changes in membrane voltage are an early mechanism necessary and sufficient to induce *Xenopus* tail regeneration. *Development* 134(7):1323–1335.
5. Martinac B, Saimi Y, Kung C (2008) Ion channels in microbes. *Physiol Rev* 88(4):1449–1490.
6. Cohen LB, Keynes RD, Hille B (1968) Light scattering and birefringence changes during nerve activity. *Nature* 218(5140):438–441.
7. Tasaki I, Watanabe A, Sandlin R, Carnay L (1968) Changes in fluorescence, turbidity, and birefringence associated with nerve excitation. *Proc Natl Acad Sci USA* 61(3):883–888.
8. Kralj JM, Douglass AD, Hochbaum DR, Maclaurin D, Cohen AE (2012) Optical recording of action potentials in mammalian neurons using a microbial rhodopsin. *Nat Methods* 9(1):90–95.
9. Kralj JM, Hochbaum DR, Douglass AD, Cohen AE (2011) Electrical spiking in *Escherichia coli* probed with a fluorescent voltage-indicating protein. *Science* 333(6040):345–348.
10. Chattoraj M, King BA, Bublitz GU, Boxer SG (1996) Ultra-fast excited state dynamics in green fluorescent protein: Multiple states and proton transfer. *Proc Natl Acad Sci USA* 93(16):8362–8367.
11. Ihara K, et al. (1999) Evolution of the archaeal rhodopsins: Evolution rate changes by gene duplication and functional differentiation. *J Mol Biol* 285(1):163–174.
12. Chow BY, et al. (2010) High-performance genetically targetable optical neural silencing by light-driven proton pumps. *Nature* 463(7277):98–102.
13. Váró G, Lanyi JK (1991) Thermodynamics and energy coupling in the bacteriorhodopsin photocycle. *Biochemistry* 30(20):5016–5022.
14. Váró G, Lanyi JK (1991) Kinetic and spectroscopic evidence for an irreversible step between deprotonation and reprotonation of the Schiff base in the bacteriorhodopsin photocycle. *Biochemistry* 30(20):5008–5015.
15. Spudich JL, Yang CS, Jung KH, Spudich EN (2000) Retinylidene proteins: Structures and functions from archaea to humans. *Annu Rev Cell Dev Biol* 16:365–392.
16. Brown LS, Dioumaev AK, Needleman R, Lanyi JK (1998) Local-access model for proton transfer in bacteriorhodopsin. *Biochemistry* 37(11):3982–3993.
17. Brown LS, Dioumaev AK, Needleman R, Lanyi JK (1998) Connectivity of the retinal Schiff base to Asp85 and Asp96 during the bacteriorhodopsin photocycle: The local-access model. *Biophys J* 75(3):1455–1465.
18. Popp A, Wolperdinger M, Hampp N, Brüchle C, Oesterhelt D (1993) Photochemical conversion of the O-intermediate to 9-*cis*-retinal-containing products in bacteriorhodopsin films. *Biophys J* 65(4):1449–1459.
19. Yamamoto N, Naramoto S, Ohtani H (1992) Photoreaction of N560 intermediate in the photocycle of bacteriorhodopsin. *FEBS Lett* 314(3):345–347.
20. Ohtani H, Itoh H, Shinmura T (1992) Time-resolved fluorometry of purple membrane of *Halobacterium halobium*. O640 and an O-like red-shifted intermediate Q. *FEBS Lett* 305(1):6–8.
21. Ohtani H, Kikuchi O (1999) Excitation spectrum of the N intermediate in the photocycle of bacteriorhodopsin. *J Phys Chem B* 103(38):8186–8188.
22. Dancshazy Z, Helgerson S, Stoeckenius W (1983) Coupling between the bacteriorhodopsin photocycle kinetics and the protonmotive force. I. Single flash measurements in *Halobacterium halobium* cells. *Photobiochem Photobiophys* 5:347–357.
23. Groma GI, et al. (1984) Coupling between the bacteriorhodopsin photocycle and the protonmotive force in *Halobacterium halobium* cell envelope vesicles. II. Quantitation and preliminary modeling of the M →bR reactions. *Biophys J* 45(5):985–992.
24. Quintanilha AT (1980) Control of the photocycle in bacteriorhodopsin by electrochemical gradients. *FEBS Lett* 117(1):8–12.
25. Geibel S, et al. (2001) The voltage-dependent proton pumping in bacteriorhodopsin is characterized by optoelectric behavior. *Biophys J* 81(4):2059–2068.
26. Nagel G, Kelety B, Möckel B, Büldt G, Bamberg E (1998) Voltage dependence of proton pumping by bacteriorhodopsin is regulated by the voltage-sensitive ratio of M1 to M2. *Biophys J* 74(1):403–412.
27. del Rosario RCH, Oppawsky C, Tittor J, Oesterhelt D (2010) Modeling the membrane potential generation of bacteriorhodopsin. *Math Biosci* 225(1):68–80.
28. Tsunoda SP, et al. (2006) H^+-pumping rhodopsin from the marine alga *Acetabularia*. *Biophys J* 91(4):1471–1479.
29. Bogomolni RA, Stubbs L, Lanyi JK (1978) Illumination-dependent changes in the intrinsic fluorescence of bacteriorhodopsin. *Biochemistry* 17(6):1037–1041.
30. Du M, Fleming GR (1993) Femtosecond time-resolved fluorescence spectroscopy of bacteriorhodopsin: Direct observation of excited state dynamics in the primary step of the proton pump cycle. *Biophys Chem* 48(2):101–111.
31. Kamiya N, et al. (1997) Picosecond fluorescence spectroscopy of the purple membrane of *Halobacterium halobium* in alkaline suspension. *Chem Phys Lett* 265(6):595–599.
32. Mukohata Y, Ihara K, Uegaki K, Miyashita Y, Sugiyama Y (1991) Australian Halobacteria and their retinal-protein ion pumps. *Photochem Photobiol* 54(6):1039–1045.
33. Ludmann K, Gergely C, Váró G (1998) Kinetic and thermodynamic study of the bacteriorhodopsin photocycle over a wide pH range. *Biophys J* 75(6):3110–3119.
34. Scherrer P, Mathew MK, Sperling W, Stoeckenius W (1989) Retinal isomer ratio in dark-adapted purple membrane and bacteriorhodopsin monomers. *Biochemistry* 28(2):829–834.
35. Stoeckenius W, Bogomolni RA (1982) Bacteriorhodopsin and related pigments of halobacteria. *Annu Rev Biochem* 51:587–616.
36. Ohtani H, Kaneko M, Ishikawa M, Kamiya N, Yamamoto N (1999) Picosecond-millisecond dual-time-base spectroscopy of fluorescent photointermediates formed in the purple membrane of *Halobacterium halobium*. *Chem Phys Lett* 299(6):571–575.
37. Zimányi L, et al. (1992) Pathways of proton release in the bacteriorhodopsin photocycle. *Biochemistry* 31(36):8535–8543.
38. Hillebrecht JR, et al. (2005) Optimization of protein-based volumetric optical memories and associative processors by using directed evolution. *NanoBiotechnology* 1:141–151.

Mechanism of voltage-sensitive fluorescence in a microbial rhodopsin

Dougal Maclaurin[*1], Veena Venkatachalam[*2], Hohjai Lee[3], Adam E. Cohen[1,3]

[(1)]*Department of Physics,* [(2)]*Biophysics program,* [(3)]*Department of Chemistry and Chemical Biology, Harvard University, Cambridge, MA 02138*
cohen@chemistry.harvard.edu

Supporting Information

Supplementary Methods

Microscope system

The single-cell data shown in Figures 2, 3, and 4 were acquired on a homebuilt microscope, illustrated in Figure S2. Beams from four CW lasers (637 nm 100 mW Coherent OBIS; 594 nm 100 mW Cobolt Mambo; 532 nm 50 mW Coherent Compass 215M; 488 nm 50 mW Omicron PhoxX) were combined using dichroic mirrors and then spectrally selected using an acousto-optic tunable filter (AOTF; Gooch and Housego 48058). White light emission from a supercontinuum laser (Fianium SC-450-6) was spectrally selected using a second AOTF (Crystal Technologies). The polarization of the CW laser outputs was rotated 90º using an achromatic half wave plate (Thorlabs AQWP05M-600), and then combined with the CW laser outputs using a polarizing beam splitter. The intensity at each wavelength was controlled with 10 µs time resolution.

Illumination was focused onto the back focal plane of the objective (Olympus, 1-U2B616 60× oil, NA 1.45) via a 650 nm long-pass dichroic mirror. The sample was illuminated in epifluorescence mode and emission was collected by the same objective and passed through the dichroic mirror. Fluorescence was filtered with a 660 – 760 nm bandpass filter (Semrock) and collected on either a photomultiplier tube (PMT; Thorlabs PMM02 with multialkali (S20) photocathode) or a cooled EMCCD camera (Andor iXon X3 860, 128 x 128 pixels). The output of the photomultiplier tube was filtered at 50 kHz using an 8-pole Bessel filter (Alligator Technologies USBPGF-S1) and recorded at 100 kS/s on a National Instruments DAQ (PCIe-6323). The DAQ also produced control waveforms for the AOTF and patch-clamp amplifier, and recorded the patch-clamp current signals.

We measured laser intensities during experiments by splitting off a small fraction of the lasers onto a photodiode (Thorlabs DET36A). We accounted for the spectral response of the photodiode by calibrating against a well-calibrated power meter (Coherent FieldMax II). Due to the nonlinear intensity dependence of Arch photophysics, it was essential to ensure uniform illumination across the sample. To achieve this we expanded the Gaussian laser beams and selected a small region in the middle using an iris in an image plane to make a sharp disk of even illumination on our sample. We confirmed using a uniform sample of fluorescent beads (Invitrogen) that the intensity did not vary by more than 10% from its mean value within this disk.

Data acquisition was controlled using custom software written in LabView (National Instruments).

Electrophysiology

Patch clamp experiments were performed at room temperature (25 °C) using an Axopatch 200B amplifier (Molecular Devices). Micropipettes were pulled from borosilicate glass capillary tubes (World Precision Instruments, 1.5 mm OD, 0.84 mm ID) using a dual-stage glass micropipette puller (Narishige, PC-10) to a tip resistance of 5-10 MΩ and filled with intracellular buffer (125 mM potassium gluconate, 8 mM NaCl, 0.6 mM $MgCl_2$, 0.1 mM $CaCl_2$, 1 mM EGTA, 10 mM HEPES, 4 mM Mg-ATP, and 0.4 mM Na-GTP at pH 7.3; adjusted to 295 mOsm with sucrose). These micropipettes were positioned using a micromanipulator (Sutter Instrument, MP-285). The extracellular solution for all recordings was Tyrode's buffer (125 mM NaCl, 2 mM KCl, 3 mM $CaCl_2$, 1 mM $MgCl_2$, 10 mM HEPES, and 30 mM glucose at pH 7.3; adjusted to 305–310 mOsm with sucrose). All patch-clamp data were acquired in voltage-clamp mode. Voltage waveforms were generated using a National Instruments DAQ (PCIe-6323) and sent to the Axopatch 200B. Currents were low-pass filtered at 10 kHz by an internal Bessel filter in the Axopatch 200B, and digitized at 50 kHz by the DAQ. Data were analyzed in MATLAB.

Preparation of Arch samples from *E. coli*

E. coli (strain BL21) were transfected with Archaerhodopsin-3 in the pET-28b vector under the T7 promoter and grown in LB containing 100 μg/mL kanamycin in a shaking incubator at 37 °C. At an OD_{600} of 0.5, protein expression was induced with 0.5 mM IPTG, and 5 μM all-*trans* retinal was added from a concentrated stock in DMSO. Cells were then returned to the incubator and grown for another four hours. Cells were harvested by centrifugation and sonicated on ice for 5 minutes in sonication buffer (150 mM TRIS, 20 mM NaCl, 5 mM $MgCl_2$, pH 7.0) using a tip sonicator. The lysate was centrifuged to collect the membranes and the supernatant was discarded. These crudely fractionated membranes were used for most experiments in the microscope. To obtain solubilized protein for transient absorption experiments, sonicated cell membranes were homogenized in a solubilization buffer (30 mM K_2HPO_4, 20 mM KH_2PO_4, 300 mM NaCl, pH 7.0, 1.5% N-Octyl-β-D-Glucopyranoside) using a glass/Teflon tissue homogenizer, and the mixture was rotated in a Falcon tube (~20 rpm) at 4 °C overnight. The detergent solubilized protein was centrifuged at 13,000 rpm for one hour; the supernatant was stored at 4°C and used for experiments within one week.

HEK cell culture

HEK293T cells were grown in DMEM supplemented with 10% FBS and penicillin/streptomycin in a 37 °C incubator under 5% CO_2. Cells were grown to 50-70% confluency in 3 cm dishes. 48 hours prior to experimentation, cells were transfected using Transit-293 (Mirus) with a WT Arch-GFP fusion construct under either the CAMKII (Addgene plasmid 22217) or ubiquitin promoter. These cells were trypsinized and re-plated at a density of ~5,000-10,000 cells/cm^2 on matrigel-coated coverglass bottom dishes (P35G-1.5-14-C, MatTek) 12 – 24 hours before experimentation. Although there is some retinal present in FBS, we added all-*trans* retinal (5 μM) to each dish 1 - 2 hours prior to imaging.

Measuring fluorescence vs. voltage

We measured Arch fluorescence as a function of membrane voltage (Fig. 2a) on HEK cells under whole-cell voltage clamp. The control voltage was a triangle wave between -150 mV and +150 mV, for 10 cycles at a sweep rate of 200 mV/s. The sweep rate was sufficiently slow that no electrical compensation was needed. We recorded fluorescence on a camera and took the average signal from a patch of membrane selected to avoid fluorescence from Arch molecules that had not trafficked to the membrane. We also subtracted background fluorescence from the coverglass and the medium by recording the same signal from a cell-free area of the dish.

The fit to a Hill curve in Figure 2a is based on a model of thermal equilibrium between two states whose energies are separated by $\alpha(V - V_0)$. The fluorescence is:

$$F = F_1 + \frac{F_2 - F_1}{1 + e^{\frac{\alpha(V-V_0)}{kT}}} \qquad \text{[S1]}$$

Where F_1 and F_2 represent the fluorescence produced by each state and αV_0 is the difference in the states' energies in the absence of applied voltage. We fitted Eq. S1 to our data on F vs. V, subject to the constraint that F_1 and F_2 must be positive, yielding α = 0.15 and V_0 = -280 mV. Allowing a 1% rms error gives bounds $0.09 < \alpha < 0.35$ and $-330 < V_0 < -50$ mV.

Measuring fluorescence response to a step in voltage

The response of Arch fluorescence to a step in voltage (Fig. 2b) was measured on HEK cells under whole-cell voltage clamp. We applied a square wave between -70 mV and +30 mV at 50 Hz, and collected the fluorescence on a PMT. The output of the PMT passed through an 8-pole Bessel filter with a cutoff of 25 kHz and was digitized at 50 kHz. The graph shows the response averaged for 1 min. Illumination was at 594 nm, 1000 W/cm^2.

A challenge in measuring fast step responses is that the membrane voltage, V_m lagged the voltage applied to the patch pipette, V_p. The capacitance of the cell membrane, C, and the series resistance of the pipette, R_p, combined to act as a low-pass filter ($R_pC \approx 0.5$ ms) on V_p. This filtering masked the true response speed of Arch. A common resolution to this problem is to use the 'compensation' circuitry in the patch clamp amplifier. The values of C and R_p are determined by observing the current produced in response to a step in V_p. The amplifier then generates a voltage waveform that exaggerates high frequency components of the desired signal to counteract the low-pass filtering of the cell.

Electrical compensation introduces some artifacts, however, because it neglects additional capacitances and resistances that lead to a more complex impulse response than can be accommodated by a simple *RC* filter. Additionally, to avoid instabilities in the amplifier, the compensation must be kept below 100%. We thus measured the step response without compensation, as shown in Figure 2b.

We modeled the response of membrane voltage V_m to a step in V_p as an exponential with time constant τ_V. This time constant was found from the relaxation time of the current in response to a step in V_p. In the experiment of Fig. 2b, τ_V = 0.4 ms. We modeled the fluorescence response of

Arch to a step in V_m as an exponential with time constant τ_F. The response of Arch fluorescence, F, expressed as a fraction of its maximum response, to a step in V_p is:

$$F(t) = \frac{1}{\tau_F}\int_0^t \left(1 - e^{\frac{-t'}{\tau_V}}\right) e^{\frac{-(t-t')}{\tau_F}} dt'$$

$$= 1 + e^{\frac{-t}{\tau_F}}\left(\frac{\tau_V}{\tau_V - \tau_F} - 1\right) - e^{\frac{-t}{\tau_V}}\frac{\tau_V}{\tau_V - \tau_F}$$

[S2]

Fitting the fluorescence to equation S2 with the single fitting parameter τ_F, we find τ_F = 0.4 ms for a step up in voltage and τ_F = 0.6 ms for a step down.

Fig. S3 shows the fluorescence step response measured using the capacitance compensation circuitry in the patch clamp amplifier. The bounce in fluorescence is an artifact of the compensation circuitry. This data also shows a time constant of 0.6 ms.

Measuring fluorescence vs. intensity

The dependence of Arch fluorescence on illumination intensity (Fig. 2c), was measured in a sample of crudely fractionated *E. coli* membranes containing Arch-eGFP. We varied the illumination intensity continuously using an AOTF. We monitored the laser power on a photodiode and the fluorescence on a PMT. Each measurement was repeated twice on the same sample region to check for sample degradation. To check for nonlinearities in the response of the photodiode or the PMT we performed the same experiment on a sample of fluorescent beads (Invitrogen). We placed neutral density filters on the excitation and emission paths to ensure that the PMT and photodiode were operating in the same range as they were during the Arch experiment. We found no nonlinearities in the electronics or detectors.

We determined the relative brightness of Arch and eGFP in a 1:1 Arch-eGFP fusion. eGFP was excited at 488 nm and emission was passed through a 531/40 bandpass filter. Arch emission was passed through a 710/100 bandpass filter. In both cases the fluorescence was collected on a PMT. The data was corrected for the wavelength dependence of the PMT quantum efficiency, which was nearly twice as high at 531 nm as at 710 nm.

Imaging sequential multiphoton excitation of Arch fluorescence in a cuvette

Figure 2d demonstrates the multiphoton character of Arch fluorescence. The data was taken in a cuvette containing detergent-solubilized Arch-eGFP. Illumination was provided by two lasers: 473 nm to excite eGFP, 594 nm to excite Arch. To ensure that the beam shape parameters were identical for both channels, the beams were expanded and then cropped by an iris at the back of the objective (Olympus, 20× NA 0.4). The image was taken using a photographic lens (Nikon, 60 mm f/2.8) and an Andor EMCCD camera (iXon3 897). The image is a composite of a white light image of the cuvette (no emission filter) mapped to the white channel, an image of Arch fluorescence (710/100 emission filter, 594 excitation, 500 1 second exposures averaged) mapped to a red channel, and an image of eGFP fluorescence (531/40 emission filter, 473 nm excitation, 60 1 s exposures averaged) mapped to a green channel.

Action spectra

The action spectra of Arch, (Fig. 2e), were collected as follows:

1. Fluorescence and voltage sensitivity spectra were obtained from HEK cells (n = 4) expressing Arch. Membrane voltage was controlled by whole-cell patch clamp. Cells were illuminated with light from a supercontinuum laser at eight evenly-spaced wavelengths between 530 nm and 635 nm (set by an AOTF), at I = 10 W/cm^2. The AOTF was calibrated with a power meter to ensure that intensity did not change across wavelengths. Each cell was illuminated for 5 s at each wavelength while the voltage cycled through the values, in mV: 0, -100, 0, +100, 0, spending 1 s at each voltage. Fluorescence was recorded on an EMCCD, and the 150 most voltage-responsive pixels (corresponding to membrane-localized Arch) were selected for analysis using the weighting algorithm described previously (1).

The fluorescence excitation spectrum was determined from the mean fluorescence at each wavelength. The voltage sensitivity spectrum was determined from the difference between the fluorescence excitation spectrum at +100 mV and the spectrum at -100 mV.

2. The absorption spectrum was acquired on detergent-solubilized Arch (in solubilization buffer at pH 7.0) using a Nanodrop 2000c (Thermo Scientific) (Fig. S5). The path length was 1 cm. To determine the absolute extinction coefficient of Arch we extracted the retinal using a method based on that of El Sayed et al. (2). Briefly, an aliquot of detergent-solubilized Arch was diluted 4x in a 2:1 chloroform:methanol solution. Retinal was cleaved from the protein by adding 20 μL of 1 M hydroxylamine. The resulting retinal oxime was collected in the chloroform fraction by shaking the sample for ~5 minutes. An absorption spectrum of the chloroform showed a peak at 362 nm, corresponding to free retinal oxime (Fig. S5). Using the extinction coefficient of retinal oxime (60,000 M^{-1}cm^{-1}), we calculated the concentration of extracted retinal oxime.

We then repeated the chloroform extraction on a sample of free retinal of known concentration (25 μM) in solubilization buffer, and measured the absorption spectrum of the extracted retinal (Fig. S5). Using the extinction coefficient of *all-trans* retinal (43,000 M^{-1}cm^{-1}), we calculated that our extraction efficiency was ~58%. Assuming a 1:1 stoichiometry of retinal binding by Arch and an extraction efficiency of 58% for retinal oxime, we determined the concentration of the original Arch sample and used this to calculate the extinction coefficient of Arch at 552 nm (ε = 50,300 M^{-1}cm^{-1}).

3. The photocurrent action spectrum was obtained from a HEK cell expressing Arch. The membrane voltage was clamped at 0 V via whole-cell patch clamp. The cell was illuminated with light from a supercontinuum laser at eight evenly-spaced wavelengths between 530 nm and 635 nm (set by an AOTF), at I = 10 W/cm^2. Exposures (1 s) alternated with darkness (1 s). The difference in membrane current between these conditions yielded the photocurrent action spectrum.

Transient absorption

Transient absorption experiments (Fig. 3a, b; Fig. 4c) were performed on a home-built apparatus. Detergent-solubilized Arch at pH 6, 7, or 8 was held in a quartz cuvette. Excitation was provided by a frequency-doubled Nd:YAG laser (Spectraphysics INDI-40) producing 5 ns pulses at 532

nm, with a 20 Hz repetition rate. We used an optical chopper to block every second pulse, so the sample saw flashes every 100 ms. White light from a 100 W Hg arc lamp (Olympus) passed through a motorized monochromator (Horiba Scientific, iHR320) then through the cuvette. The transmitted light was recorded on a photodiode (Thorlabs, DET36A) and digitized at 100 kHz on a National Instruments DAQ (PCIe-6259). We recorded for 5 s (50 pump cycles) at each wavelength, and cycled through the wavelengths 20 times.

We recorded absorption for every pump pulse, only averaging in post-processing, so that we could check for degradation of the sample. We saw some bleaching of the sample but the shape of the spectra did not change with time. We also recorded the photodiode signal with each of the beams (pump and probe) independently shuttered to check for electrical artifacts. We varied the pump intensity to ensure that the signal was linear in pump intensity.

Fitting transient absorption data

We fit the transient absorption data in Fig. 2b to exponential curves of the form

$$I(\lambda, t) = \sum_{i=1}^{n} B_i(\lambda) e^{\frac{-t}{\tau_i}} \quad [S2]$$

At 400 nm and 560 nm, the absorption vs. time traces were fit to this equation with n = 3 to determine the rates (*"τ"*) and weights (*"B"*) shown in Table S1. The first two time constants from this fit were held as fixed parameters when fitting the absorption vs. time at 640 nm to an equation of the same form (with n = 4, τ_1 = .04 ms, and τ_2 = .39 ms). The rates and weights from this fit are shown in Table S1. The fits to the data at all three wavelengths are plotted as black lines in Figure 3b.

	τ_1 = .04 ms	τ_2 = .39 ms	τ_3 = 4.1 ms	τ_4 = 14.3 ms	τ_5 > 100 ms
400 nm	-1.7	4.8	*n/a*	*n/a*	.5
560 nm	1.7	-5.3	*n/a*	*n/a*	-3.9
640 nm	.30	-.34	-.65	.90	*n/a*

Table 1. Weights ($B_i \times 10^3$) of indicated components from fitting transient absorbance data in Figure 2b to Eq. S2 with n = 3 (400 nm, 560 nm) or n = 4 (640 nm).

Transient fluorescence

Transient fluorescence measurements (Fig. 3c) were performed on crudely fractionated *E. coli* membranes containing Arch, in our home-built microscope. Pump pulses were 532 nm, 50 W/cm^2, and lasted 100 μs. To minimize the perturbation due to the probe, we used dim red probe pulses (640 nm, 15 W/cm^2), and only recorded fluorescence during the first 20 μs of the probe pulse. We verified that the fluorescence signal was linear in probe intensity. We waited 150 ms between pump pulses. Waiting longer did not affect the data.

Each data point represents the average of 30 pump-probe cycles. PMT and photodiode signals were filtered at 50 kHz and digitized at 100 kHz. The raw data traces showed negligible sample degradation during these experiments.

The triple pulse (pump-pump-probe) scheme provides rich information on light-driven transitions of photocycle intermediates, and the lifetimes of the resulting states. In addition to the data shown in Fig. 3c we varied the intervals between pulses (Figure S9), the wavelength of each pump (Figure S10) and the intensity of each pump (Figure S11).

Confocal scan

Figure 3e shows four images taken on a commercial scanning confocal microscope (Zeiss LSM 710) of a HEK293T cell expressing an Arch-eGFP fusion. Arch was excited at 594 nm and eGFP was excited at 488 nm. The scan rate was 0.47 ms per line. The 'line scan' mode scanned each line 16 times before moving on to the next line whereas the 'frame scan' mode scanned the entire field of view, line-by-line, and repeated 16 times.

Time- and voltage-dependent fluorescence in HEK cells

Time-dependent fluorescence and photocurrent (Fig. 4a, b, d) were measured in single HEK cells expressing Arch under whole-cell voltage clamp.

To investigate the fluorescence response to onset of illumination at different voltages (Fig. 4a), the membrane potential was set to -100 mV or +100 mV via whole cell patch clamp. The cell was exposed to a pulse of light (50 ms, 594 nm, 1000 W/cm^2) followed by 250 ms of darkness and the fluorescence was recorded (Fig. 4a). The cycle was repeated 10 times. Average fluorescence responses show that fluorescence and voltage sensitivity arose several milliseconds after onset of continuous illumination.

To investigate the fluorescence response to a brief flash of light (Fig 4b, F and ΔF), we initiated the photocycle with a flash (1000 W/cm^2, 100 μs, 594 nm), and then probed the fluorescence with a second flash (1000 W/cm^2, 100 μs, 594 nm) with variable delay, *t*. Each data point is the average of 80 pump-probe measurements. To measure F, the membrane voltage was clamped at V_m = 0. To measure ΔF, the membrane voltage was held fixed at +30 mV and then at -70 mV.

The probe flashes were sufficiently intense to drive $N \rightarrow Q$ and to excite fluorescence of *Q*, i.e. to provide photons 2 and 3 in the scheme of Fig. 3d. Intense probe beams were necessary for the single-cell measurements due to the much smaller sample volume compared to the experiments on fractionated *E. coli* membranes. The fluorescence measured at the single-cell level peaked at *t* = 5 ms, similar to that measured in bulk (Fig. 3c(iii)). Considering the different protein environments (crudely fractionated *E. coli* membranes vs. intact HEK cells), we do not consider the difference in timing to be significant.

To investigate the effect of violet flashes on steady-state fluorescence and photocurrent at different voltages (Fig. 4d, S13), the membrane potential was varied in steps of 30 mV from -90 mV to +60 mV. At each voltage, pulses of red light were applied to elicit steady-state fluorescence and photocurrent (100 ms, 640 nm, 4000 W/cm^2). 54 ms after turning on the red light, a short pulse of violet light (11 ms, 407 nm, 40 W/cm^2) was applied to the cell to perturb steady-state fluorescence and photocurrent. The red light was turned off for 100 ms between red pulses. This procedure was repeated four times at each voltage. Background fluorescence due to the 407 nm light alone was subtracted from fluorescence measurements.

Ground-state recovery probed by two-pulse photocurrent

The integrated photocurrent following a brief pulse of light provides a measure of the ground state population of Arch. By measuring this photocurrent under a two-pump protocol with variable delay, we probed the duration of the photocycle.

HEK cells expressing Arch were held at a membrane voltage of 0 mV via whole cell patch clamp. Cells were exposed to two flashes of light (100 μs, 594 nm, 1000 W/cm^2) with variable delay, t_{probe}. Membrane current was recorded continuously. The protocol was repeated at 600 ms intervals.

Transient capacitance measurements

A voltage-dependent equilibrium between differently charged states should manifest as an increase in membrane capacitance. If this equilibrium only occurs at a certain time in the photocycle, then one expects to detect a time-dependent capacitance subsequent to a flash of light. To measure time-dependent capacitance (Fig. 4b), we set $V_m = V_0 + A\sin(2\pi ft)$, with V_0 = -25 mV, A = 35 mV and f = 1 kHz. We recorded the current while flashing light every 400 ms (100 μs flashes, 532 nm, 500 W/cm^2).

Here we discuss how to calculate this time-dependent capacitance from time-resolved AC electrical impedance measurements. We modeled the cell by the circuit shown in Figure S14, consisting of the pipette resistance, R_p (≈ 20 MΩ), the membrane resistance, R_m (≈ 500 MΩ), and the membrane capacitance, C (≈ 20 pF). We applied a 1 kHz AC voltage $V(t)$ = Re($Ve^{i\omega t}$) and recorded the current.

Allowing for time-dependent capacitance, the dynamics of the circuit are described by

$$i = \frac{V_m}{R_m} + \frac{dV_m}{dt}C + V_m\frac{dC}{dt} \qquad \text{[S3a]}$$

$$i = \frac{V - V_m}{R_p} \qquad \text{[S3b]}$$

where V_m is the voltage across the membrane. Eq. S3a has an important difference from the usual description of time-dependent current in an electric circuit. Usually, the relation $Q = CV$ leads to the time-dependent expression $i = C\frac{dV}{dt}$. However, in a circuit where the capacitance may change on the same timescale as the voltage, one must include an additional contribution to the current, $V\frac{dC}{dt}$.

We made two simplifying assumptions: 1) the membrane resistance was large compared to the impedance of the membrane capacitance ($R_m >> 1/(\omega C)$) and 2) the capacitance changed slowly relative to the frequency of the applied voltage. This second approximation is almost certainly not true early in the photocycle, but is likely to be true on timescales long compared to the period of the probe voltage (1 ms in the present experiment), because molecular dephasing suppresses the effects of fast transitions late in the photocycle. With these approximations, we can ignore the term $V_m\dot{C}$ and estimate $C(t)$ as:

$$C(t) = \frac{-1}{\omega \mathrm{Im}[\tilde{V}(t)/\tilde{I}(t)]} \qquad \text{[S4]}$$

In Eq. S4, $\tilde{V}(t)$ and $\tilde{I}(t)$ are the Fourier components of voltage and current at the driving frequency, defined with the Fourier integral performed over a single period, Δt.

$$\tilde{V}(t) = \int_{t-\Delta t/2}^{t+\Delta t/2} e^{-i\omega t'} V(t') dt',$$

and similarly for $\tilde{I}(t)$.

Interpretation of transient capacitance

Here we relate transient capacitance to molecular parameters using a simple model. Consider an equilibrium between two states of Arch whose substantial difference is the position of a single charge (a proton, say) as shown in Figure S14. A voltage V_m applied to the membrane shifts the relative energies by an amount $V_{eff} = \alpha(V_m - V_0)$, where α represents the fraction of total membrane voltage drop that occurs between the two possible charge locations. V_0 is the membrane voltage at which the states have equal energy. The probability of populating state 1, in terms of the effective voltage V_{eff}, is given by the Boltzmann distribution:

$$p = \frac{1}{1 + e^{\frac{-eV_{\mathrm{eff}}}{kT}}}$$

This system acts as a capacitor in that the distribution of charges is a function of voltage. Near $V_{eff} = 0$, the capacitance is given by:

$$C = \frac{dQ}{dV_{eff}} = e\frac{dp}{dV_{eff}} = \frac{e^2}{4kT} = 1.6 \times 10^{-18}\ \mathrm{F}. \qquad \text{[S5]}$$

How does this capacitance affect the capacitance of the membrane? The charge is capacitively coupled to the conducing regions on either side of the membrane as shown in Figure S14. The contribution to the total capacitance will depend on α, the fraction of the membrane voltage drop which occurs between the two charge locations. This fraction must also be the ratio of the two capacitances C_1 and C_2 shown in Figure S14. The contribution of the voltage-dependent equilibrium of a single Arch molecule to the total membrane capacitance is therefore:

$$\Delta C = \alpha^2 \frac{e^2}{4kT}. \qquad \text{[S6]}$$

Our measurement of transient capacitance yielded $\Delta C/N = 1.7 \times 10^{-20}\mathrm{F}$, where N is the number of molecules of Arch in the membrane, determined by transient photocurrent (see below). These results give $\alpha = 0.1$. This measurement is in fair agreement with the estimate $0.09 < \alpha < 0.35$ determined by fitting a Hill curve to our fluorescence versus voltage data, especially considering the very different nature of these two measurements.

Estimate of density of Arch molecules

We obtained an estimate of the areal density of Arch molecules by considering the photocurrent following a pulse of light. The integrated charge displacement after a pulse of 50 W/cm^2 for 100 μs was 1.1 pC, or 7×10^6 protons. Based on the photocurrent saturation curve (Fig S4) we estimate 50% activation of Arch under these illumination conditions. We thus estimated the total number of Arch molecules in the plasma membrane to be $N = 1.4 \times10^7$. For the same cell, the capacitance measurement described above yielded a membrane capacitance of 41 pF. Assuming a membrane capacitance of 1 μF/cm^2, gives approximately 3500 Arch molecules per square micron.

Model of voltage-dependent fluorescence in Arch

We modeled the photocycle of Figure 2e quantitatively. We assigned rates to each transition in this model: k_{GM} = ground to *M* under red illumination (with no red light, $k_{GM} = 0$); $k_{NG} = N$ to ground; $k_{MG} = M$ to ground under violet illumination (with no violet light, $k_{MG} = 0$). We assigned fractional charge movements to each forward transition in the model (Q_{GM} and Q_{NG}) such that the total charge moved in the photocycle is 1 ($Q_{GM} + Q_{NG} = 1$), and we assumed that the charge movement from ground to M is equal and opposite to the charge movement from *M* to ground ($Q_{GM} + Q_{MG} = 0$). We assumed that *M* and *N* equilibrate quickly to an equilibrium given by $K(V)$ satisfying a two-state Boltzmann distribution:

$$K(V) = e^{\frac{\alpha(V-V_0)}{k_B T}}$$

We further assumed that fluorescence was proportional to the population of *N*, with proportionality constant F_1 allowing for a small constant background fluorescence, F_0. The populations evolve according to:

$$M = N/K$$

$$\frac{d}{dt}\begin{bmatrix}G\\N\end{bmatrix} = \begin{bmatrix}-k_{GM} & k_{NG} + k_{MG}/K\\ k_{GM}K/(K+1) & -k_{NG}K/(K+1) - k_{MG}/(K+1)\end{bmatrix}\begin{bmatrix}G\\N\end{bmatrix}$$

while the fluorescence *F* and current *I* are given in terms of the states' populations:

$$F = F_0 + F_1 N$$

$$I = I_1(Q_{GM}k_{GM}G - Q_{GM}k_{MG}M + Q_{NG}k_{NG}N)$$

where I_1 is the constant of proportionality equal to the number of molecules in the membrane.

We solved for the N population after the onset of illumination:

$$N(t) = \frac{\left(1 - e^{-\frac{(\mathrm{k_{MG}} + \mathrm{k_{GM}} + K(\mathrm{k_{NG}} + \mathrm{k_{GM}}))t}{1+K}}\right) K\mathrm{k_{GM}}}{\mathrm{k_{MG}} + \mathrm{k_{GM}} + K(\mathrm{k_{NG}} + \mathrm{k_{GM}})}$$

which reduces to the following under steady-state illumination (t = ∞):

$$N = \frac{K\mathrm{k_{GM}}}{\mathrm{k_{MG}} + \mathrm{k_{GM}} + K(\mathrm{k_{NG}} + \mathrm{k_{GM}})}$$

Fluorescence and current were calculated using the equations given above under both steady-state illumination and as a function of time after the onset of red illumination (k_{MG} = 0). This model was able to reproduce the main features of the data shown in Figure 4(d) using the following parameters: k_{GM} = .5 ms^{-1}, k_{NG} = .033 ms^{-1}, k_{MG} = .2 ms^{-1}, Q_{GM} = 0.09, α = 0.35, and V_0 = -30 mV. The fits resulting from using these parameters are shown in Fig. S13.

Supplementary Figures

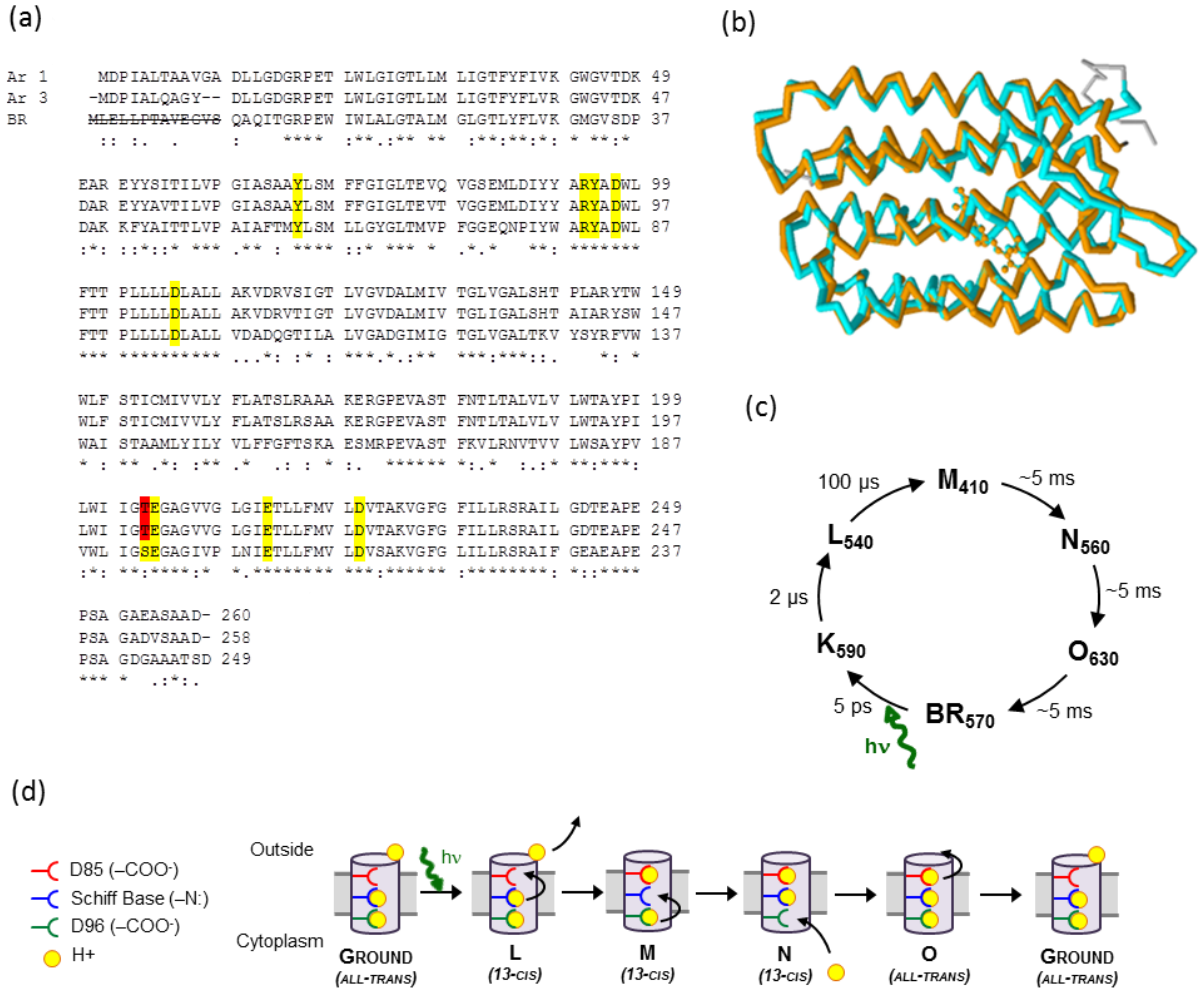

Figure S1. Comparison of Arch-3, Arch-1, and Bacteriorhodopsin. (a) Sequence alignment via ClustalW2. Arch-1 (Uniprot P69051) and Arch-3 (Uniprot P96787) share 93% amino acid identity. Arch-3 and BR share 61% amino acid identity. All key residues in the proton-pumping pathway (yellow) are shared except for S193 in BR (T203 in Arch-3). This residue is part of the extracellular proton release group. The first 13 amino acids of BR are removed in a posttranslational modification. BR residue numbering has been adjusted to reflect spectroscopic convention. (b) Structural alignment of Arch-1 (pdb 1UAZ) (3) with BR (pdb 1FBB) by jFATCAT. No structural adjustment was allowed. The RMSD between the structures was 1.07 Å. (c) Simplified version of the BR photocycle with absorption maxima of each state, adapted from (4). (d) Simplified cartoon of one cycle of the BR photocycle (omitting the short-lived K state and ignoring back-reactions and branches) showing how a proton moves from the cytoplasmic side to the extracellular side. In BR, D85 is the proton acceptor, and D96 is the proton donor. These residues correspond to D95 and D106, respectively, in Arch-3.

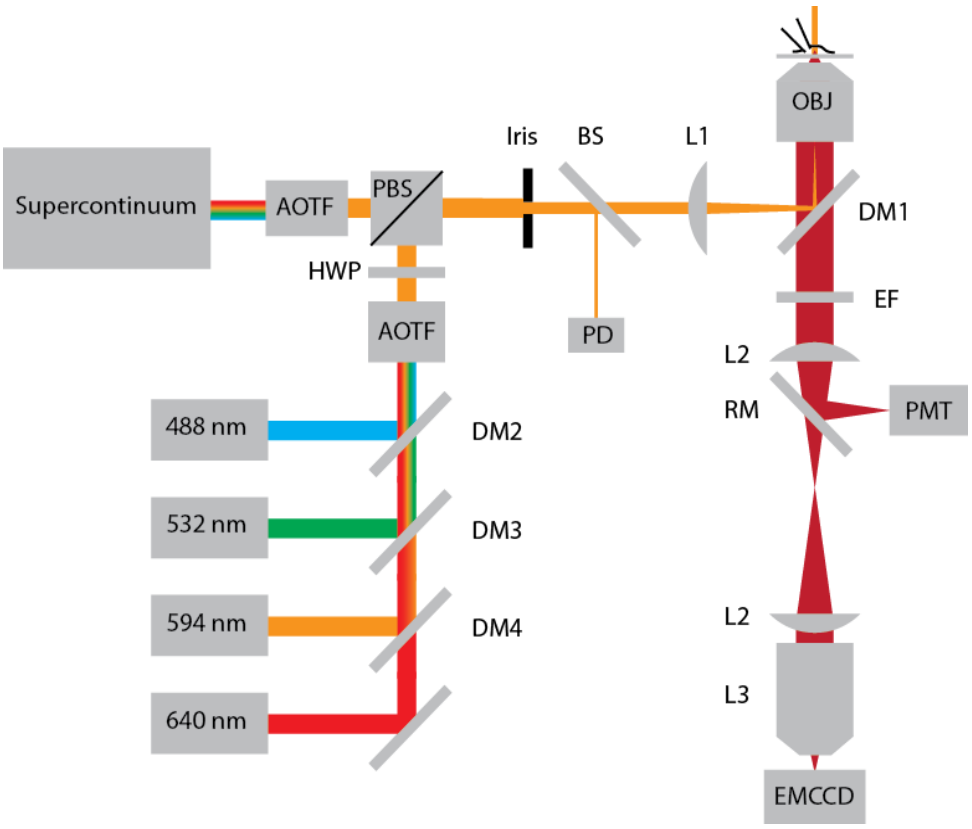

Figure S2. Schematic diagram of home-built microscope. AOTF: acousto-optic tunable filter. EMCCD: elctron-multiplying charged-coupled device camera. PMT: photmultiplier tube. OBJ: Objective lens. EF: emission filter. DM(1-4): dichroic mirror. PBS: polarizing beam splitter. HWP: half-wave plate. PD: photodiode. BD: beam splitter. L1, L2 achromatic lenses. L3: photographic lens. RM: removeable mirror.

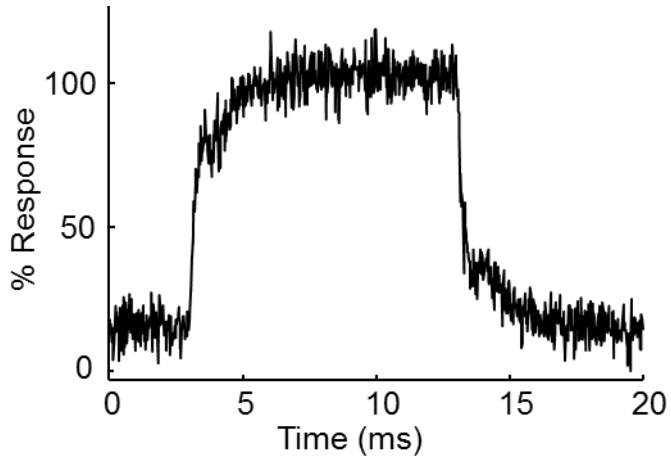

Figure S3. Compensated fluorescence step response. Fluorescence response to a step in voltage between -70 mV and +30 mV similar to that shown in Figure 2b, but with patch-clamp amplifier compensation circuitry enabled. The initial fluorescence response reflects the intrinsic response time of Arch. The bounce in fluorescence is an artifact of the compensation circuitry.

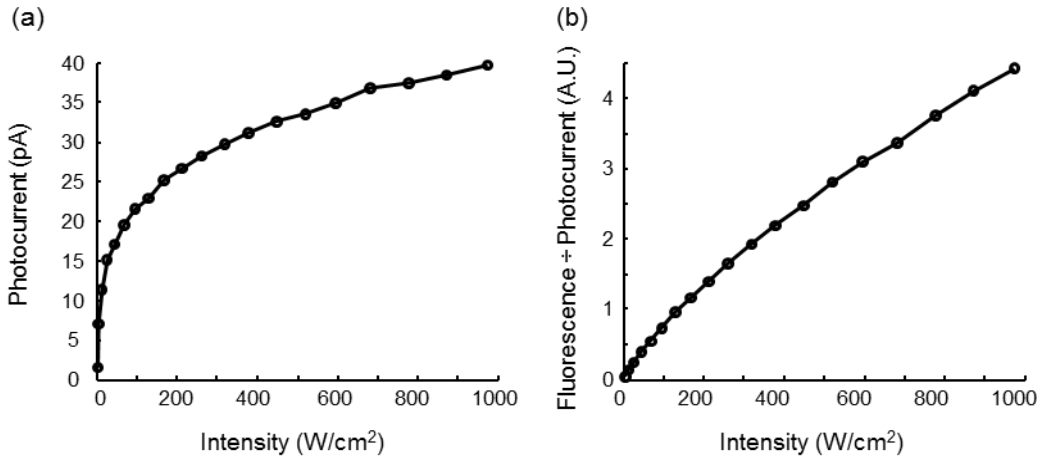

Figure S4. Saturation of Arch photocurrent at 594 nm. (a) Steady-state photocurrent in a HEK cell expressing Arch, as a function of illumination intensity at 594 nm. Membrane voltage was held at 0 mV by whole-cell patch clamp. The cell was alternately exposed to 50 ms of illumination and 50 ms of darkness. The plot shows the average difference in membrane current between these conditions. Each data point represents the average of 6 measurements. (b) Fluorescence per pA of photocurrent, recorded on the same cell as in (a). At higher illumination intensity, the fluorescence signal grew superlinearly, while the photocurrent saturated. Thus fluorescence measurements yield maximum signal relative to perturbation to membrane potential when the illumination was concentrated on a small piece of a cell. If fluorescence and photocurrent were both linear in illumination intensity, the graph in (b) would be a horizontal line.

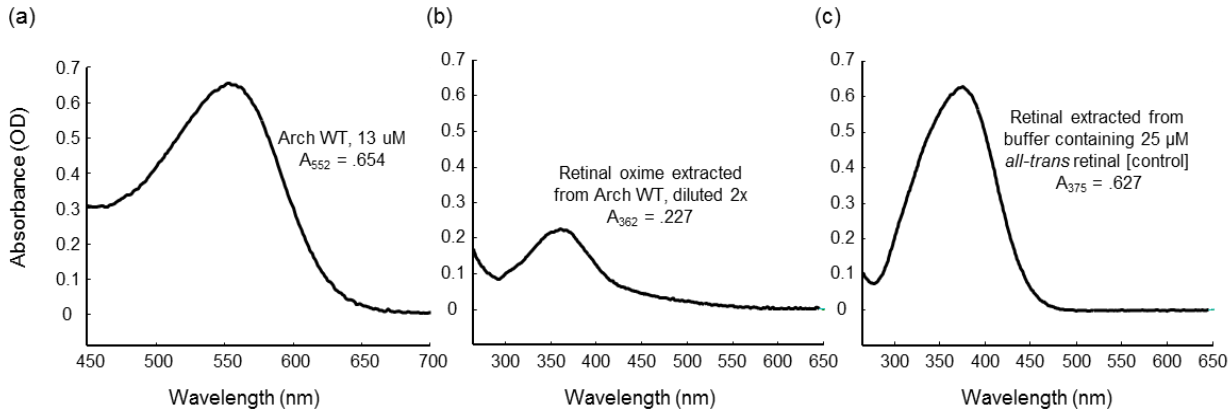

Figure S5. Determination of the extinction coefficient of Arch. (a) Absorption spectrum of detergent-solubilized Arch, pH 7 (b) Absorption spectra of retinal oxime extracted from the sample in (a). (c) Absorption spectrum of retinal extracted from a reference sample of known concentration.

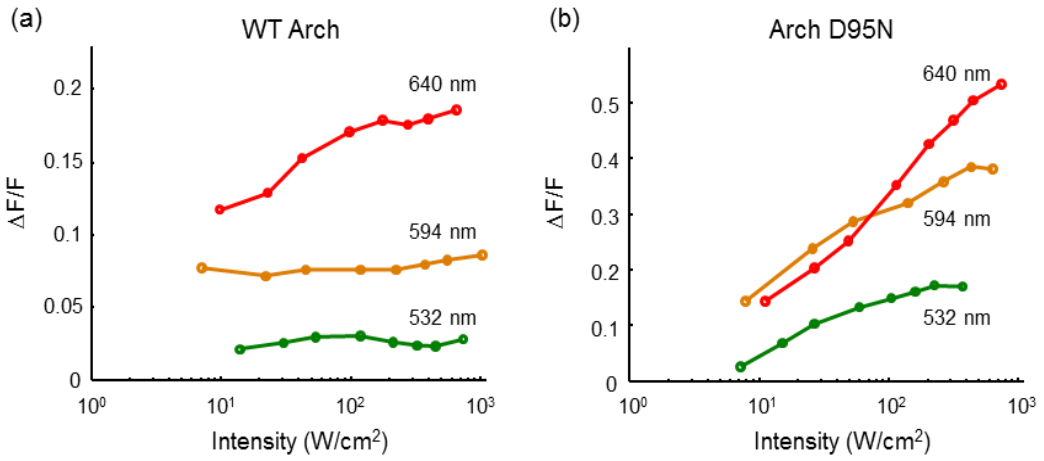

Figure S6. Voltage sensitivity vs. illumination intensity for Arch and Arch(D95N). (a) Voltage sensitivity (ΔF/F) of Arch WT increased nearly two-fold between 10 W/cm^2 and 650 W/cm^2 under illumination at 640 nm, while voltage sensitivity was independent of illumination intensity under illumination at 532 nm and 594 nm. Note that the parameter plotted here, ΔF/F, is different from the absolute change in fluorescence, ΔF, which is plotted in Figure 2e. (b) In contrast, the voltage sensitivity of Arch D95N increased markedly with illumination intensity at all three wavelengths. Sensitivity increased 5x between 10 W/cm^2 and 700 W/cm^2 at 640 nm. These results imply that fluorescence of Arch WT is dominated by a single fluorescent species, with possibly a weak contribution from a red-shifted voltage-insensitive state. Fluorescence of Arch(D95N) appears to have contributions from voltage sensitive and insensitive states, with the photostationary equilibrium shifting toward the voltage sensitive state(s) at higher illumination intensity.

HEK cells expressing Arch WT or Arch(D95N) were subjected to whole-cell voltage clamp and exposed to illumination of specified wavelength and intensity. Fluorescence was recorded on an EMCCD. At each wavelength, intensity was increased in steps (1.6 seconds per step) from 0 to ~800 W/cm^2. At each intensity, membrane voltage was stepped between -70 mV and +30 mV four times at a frequency of 2.5 Hz. The entire waveform was repeated 2x per cell to ensure stability of the system. ΔF/F was calculated as the change in fluorescence over 100 mV (between -70 mV and +30 mV) divided by the fluorescence at -70 mV of the 150 most responsive pixels (as determined using the weighting algorithm outlined by Kralj *et al*. (1)). In (a) and (b) data is averaged over n = 2 cells.

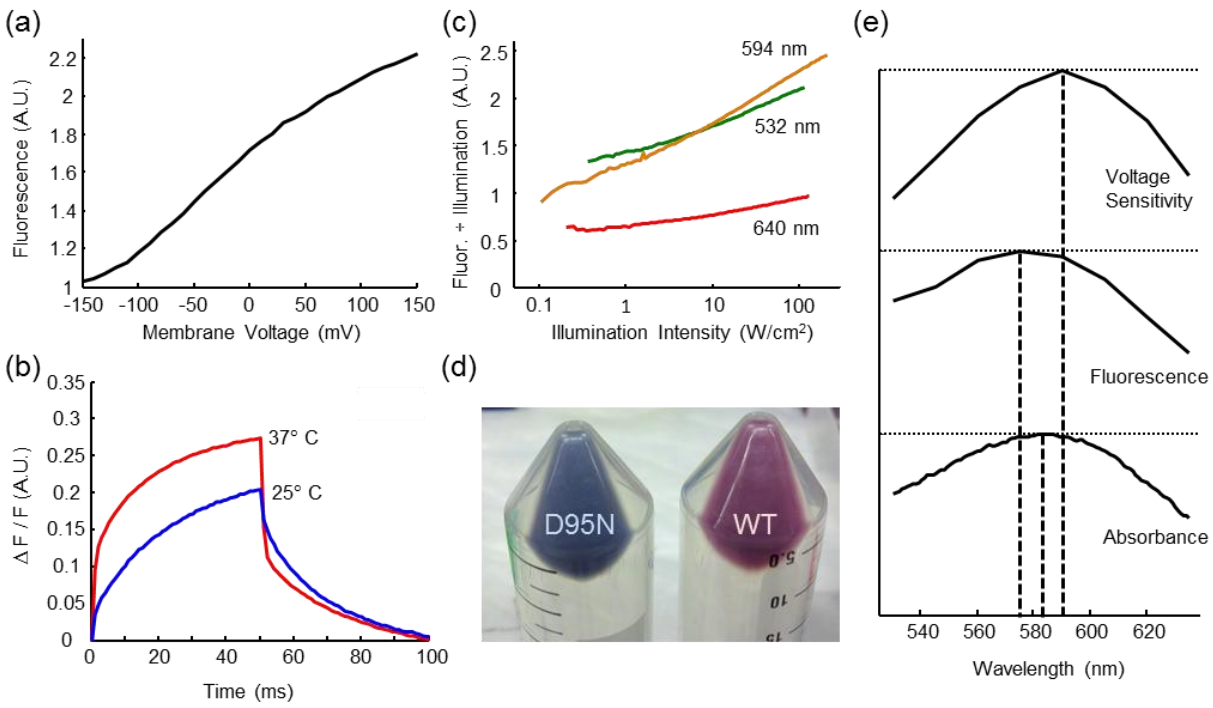

Figure S7. Characterizing Arch(D95N). (a) Voltage-sensitive fluorescence of Arch(D95N) (exc. 594 nm, 1000 W/cm^2, em. 660 – 760 nm) in HEK cells at 25 °C. Membrane voltage was controlled via whole-cell patch clamp. Fluorescence was recorded on an EMCCD camera. (b) Fluorescence response to a voltage step between -80 mV and +20 mV at two temperatures. (c) Ratio of fluorescence to illumination intensity (*F*/*I*), as a function of illumination intensity, showing the nonlinear response of Arch(D95N) fluorescence. (d) Picture of *E. coli* expressing Arch(D95N) (left, blue) and Arch (right, purple), demonstrating the difference in ground-state absorption spectra of these two species. (e) Action spectra for Arch(D95N) (analogous to those obtained for WT Arch in Figure 2(e)). Arch(D95N) did not generate a detectable photocurrent.

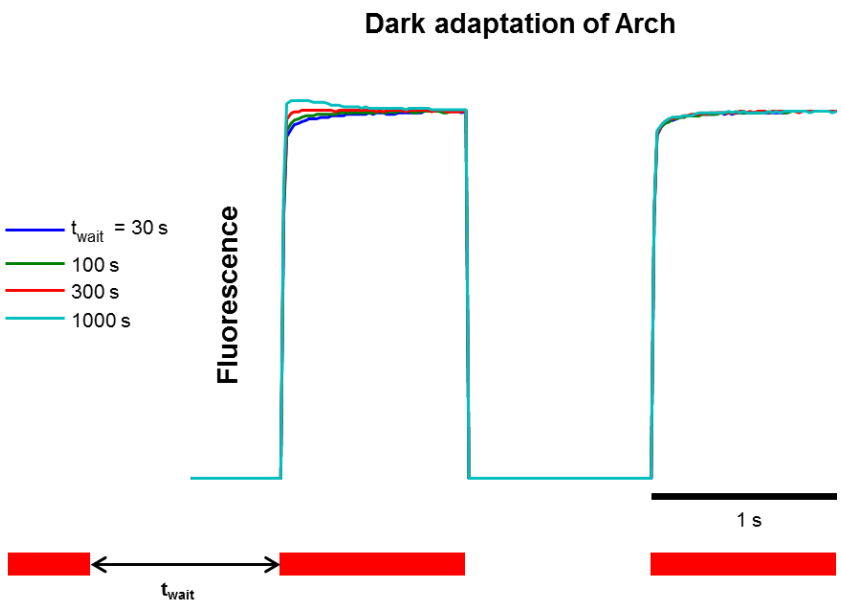

Figure S8. Dark adaptation of Arch. Arch was expressed in *E. coli* as described previously and illuminated with two pulses of red light (637 nm, 200 W/cm^2) as shown. The sample was then left in the dark for some duration t_{wait} and the sequence was repeated. The initial fluorescence during the first pulse depended on the time (t_{wait}) since the previous pulse, demonstrating that Arch underwent a very slow (~ 5 minutes) change in the dark.

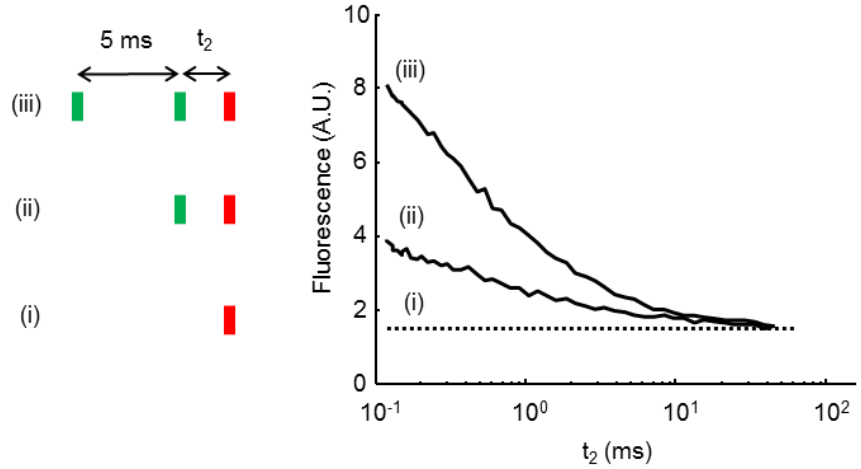

Figure S9. Nonlinear fluorescence properties of Arch. Decay of the fluorescent *Q* state. Fluorescence was recorded as a function of the delay between the last pump pulse and the probe. Illumination and recording conditions were as in Fig. 3c. Curve (i) shows the low fluorescence of the ground state. Curve (ii) shows that a single pump pulse created a small fluorescent population which decayed in 1.0 ms. Curve (iii) shows the decay of the fluorescent *Q* state created by two sequential pump pulses 5 ms apart. The *Q* state decayed in 0.84 ms. The similar decay rates in curves (ii) and (iii) led us to conjecture that they reflect the same state, i.e. that there exists a small population in the pre-fluorescent *N* state in Arch in the dark.

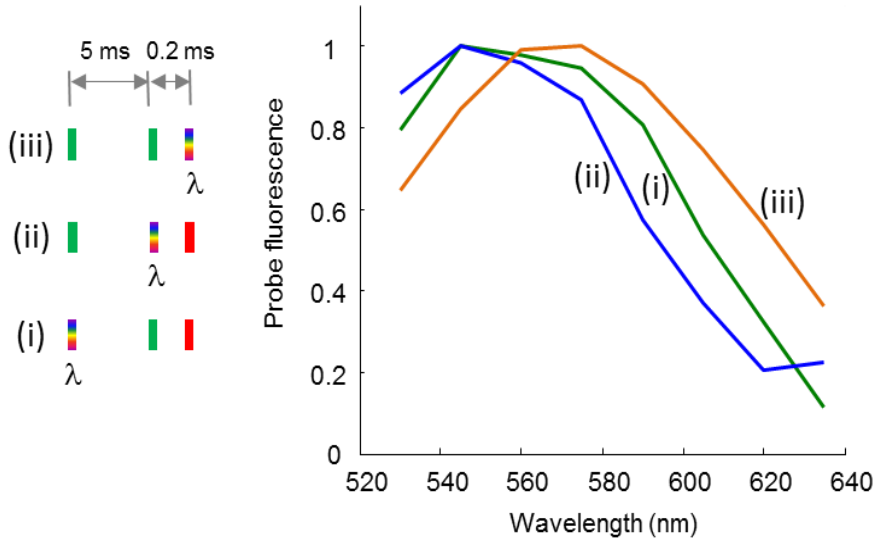

Figure S10. Action spectra of each photon-mediated transition. We determined the spectrum of each photon-mediated transition by varying the wavelengths of each illumination pulse while keeping the other pulses fixed. The initial fluorescence elicited by the final pulse is plotted as a function of the wavelength of either the first (i), second (ii), or third (iii) photon.

Illumination and recording conditions were as in Fig. 3c. The variable-wavelength pulses were at an intensity of 0.7 W/cm^2 and were obtained from the supercontinuum laser. The fixed-wavelength pulses were at 532 nm, 50 W/cm^2 for pumps 1 and 2, and 640 nm, 15 W/cm^2 for the probe pulse. All pulses were 100 μs long. Fluorescence was determined from the first 20 μs of the probe pulse to ensure that the probe did not perturb the state of the protein. We verified that fluorescence was linear in the probe intensity.

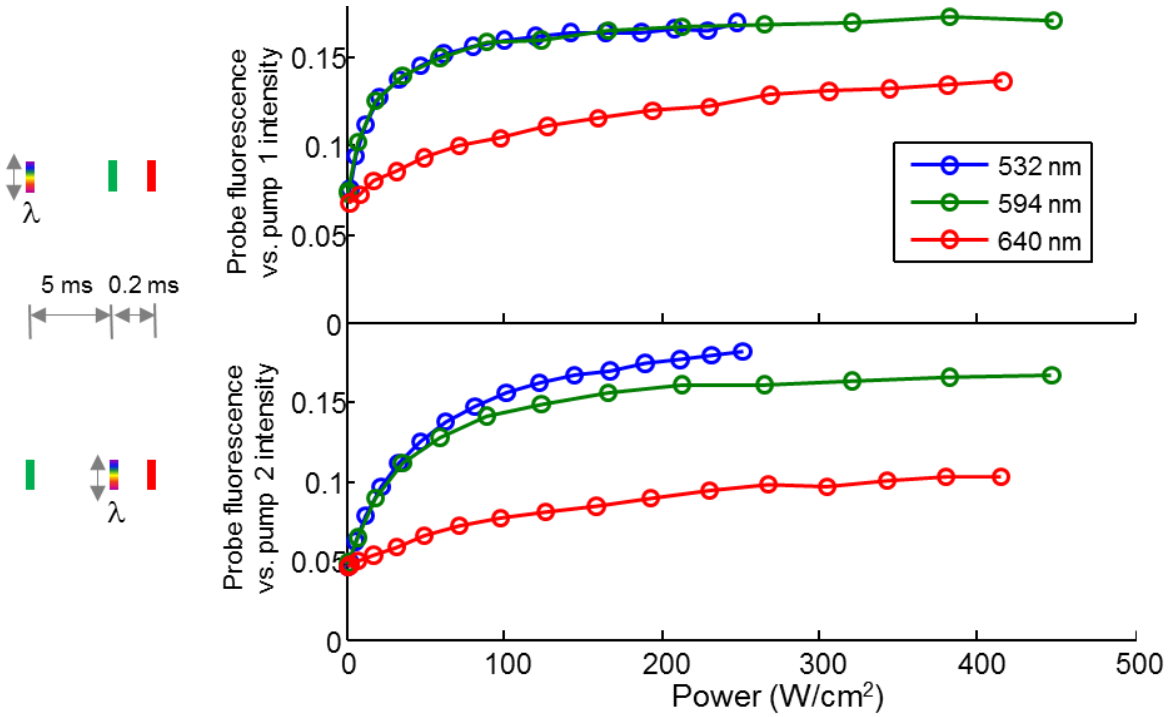

Figure S11. Saturation of the first two photon-mediated transitions. We varied the intensity of pumps 1 and 2 to measure the saturation of these optically driven transitions. In all cases the pumps were 100 μs long and the fixed-intensity pump was at 532 nm, 50 W/cm^2. When the pump wavelength was 640 nm, the saturation value of the fluorescence was lower than when the pump wavelength was 594 nm or 532 nm. This was true for both the first and second pumps. These results suggest a possible back-reaction or non-pumping shortcut in the photocycle with a red-shifted action spectrum. We did not detect saturation of the third pulse (the pulse responsible for exciting fluorescence). Due to the extremely short excited state lifetime of *Q* (~62 ps in BR), this state is expected to saturate at experimentally inaccessible intensities.

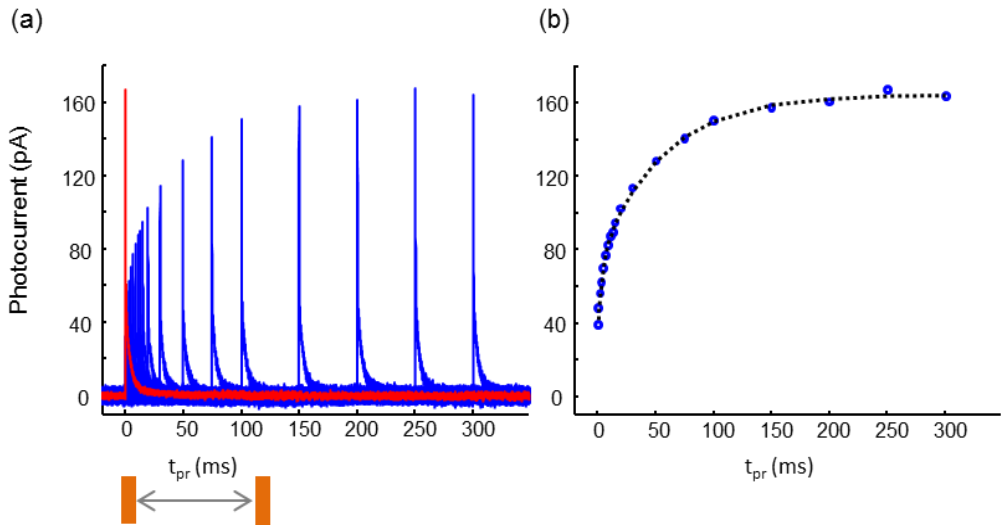

Figure S12. Ground state recovery measured by photocurrent in HEK cells. We measured the time-course of ground state recovery in HEK cells by monitoring the photocurrent recovery in a two-pulse experiment. (a) Current due to the first illumination pulse (red). Additional current due to each probe pulse (blue). (b) Peak photocurrents from the second pulse (blue circles). Fit to a double exponential (black dotted line) with time constants of 3.8 ms (weighting coefficient = 1) and 54 ms (weighting coefficient = 3). When photocurrent recovery was fit to a single exponential, the time constant was 32 ms.

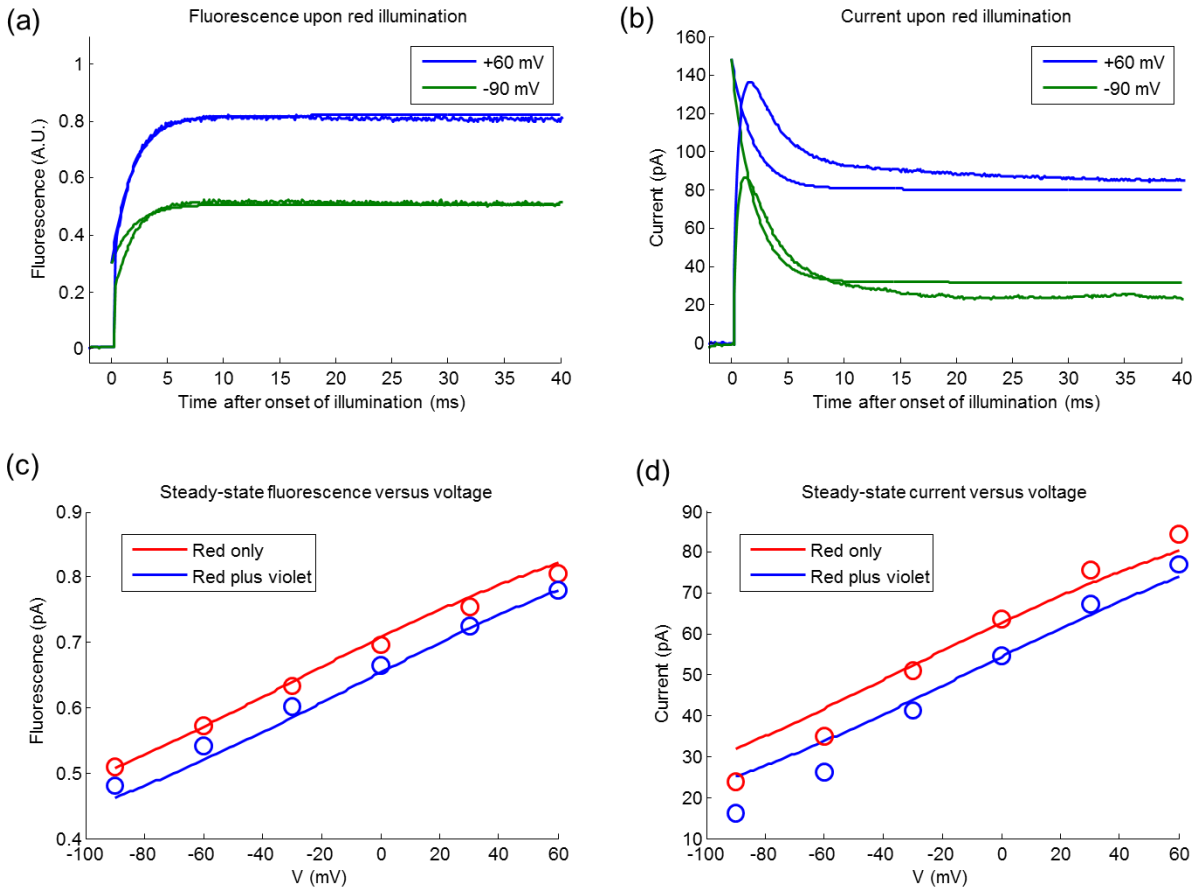

Figure S13. Fits to the photocycle in Figure 4e. We modeled the photocycle of Figure 2e quantitatively (see "Model of voltage-dependent fluorescence in Arch" in Supplementary Methods)**.** We reproduced the main features of the data shown in Figure 4d. Panels (a) and (b) show the response of fluorescence and current to the onset of red illumination at -90 mV and +60 mV (see "Time- and voltage-dependent fluorescence in HEK cells" in Methods for experimental details). Fits are shown. The model reproduced the shapes of the transients in both fluorescence and current upon illumination onset. Panels (c) and (d) show steady-state fluorescence and current as a function of membrane voltage under constant 640 nm illumination and under 640 nm + 407 nm illumination. The voltage-dependence of both fluorescence and photocurrent, as well as the decreases in fluorescence and current caused by 407 nm illumination, were recapitulated by our model.

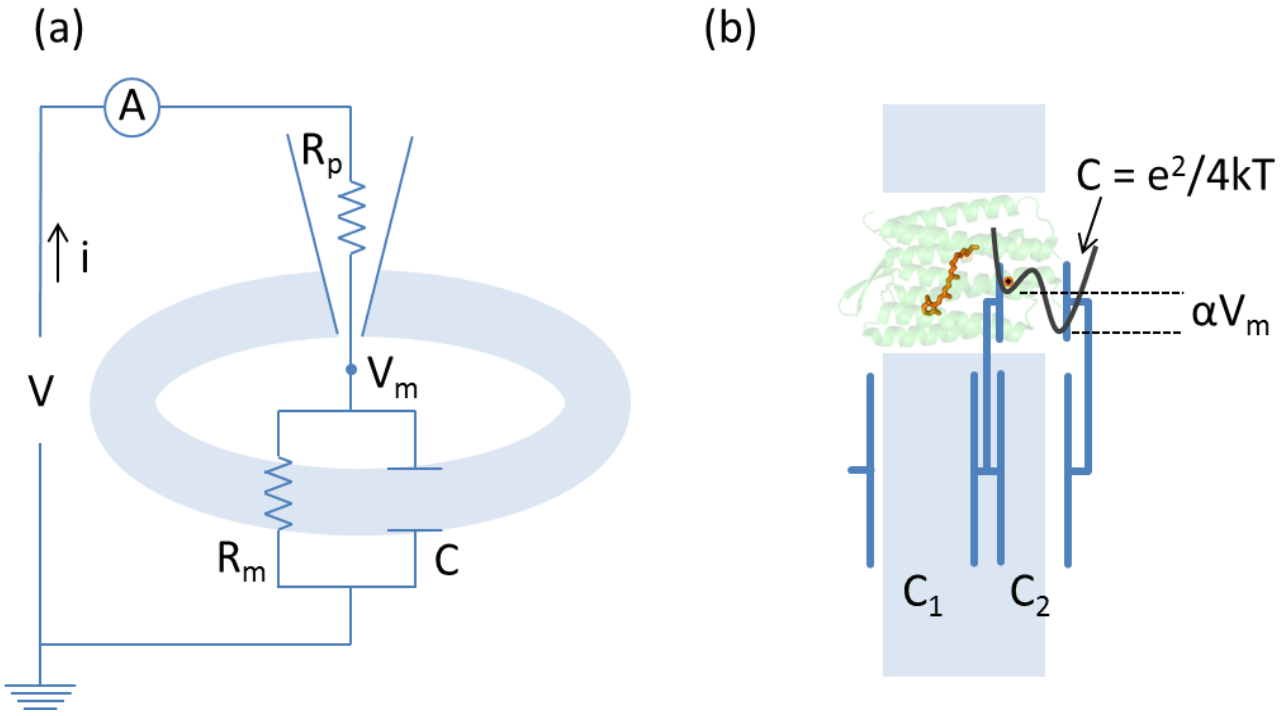

Figure S14. Electrical models of transient capacitance data. (a) Equivalent circuit of a cell under patch clamp, showing the pipette resistance, R_p, the membrane capacitance, C, and the membrane resistance, R_m. (b) Voltage-dependent equilibrium of Arch contributes to membrane capacitance by providing a voltage-dependent charge distribution.

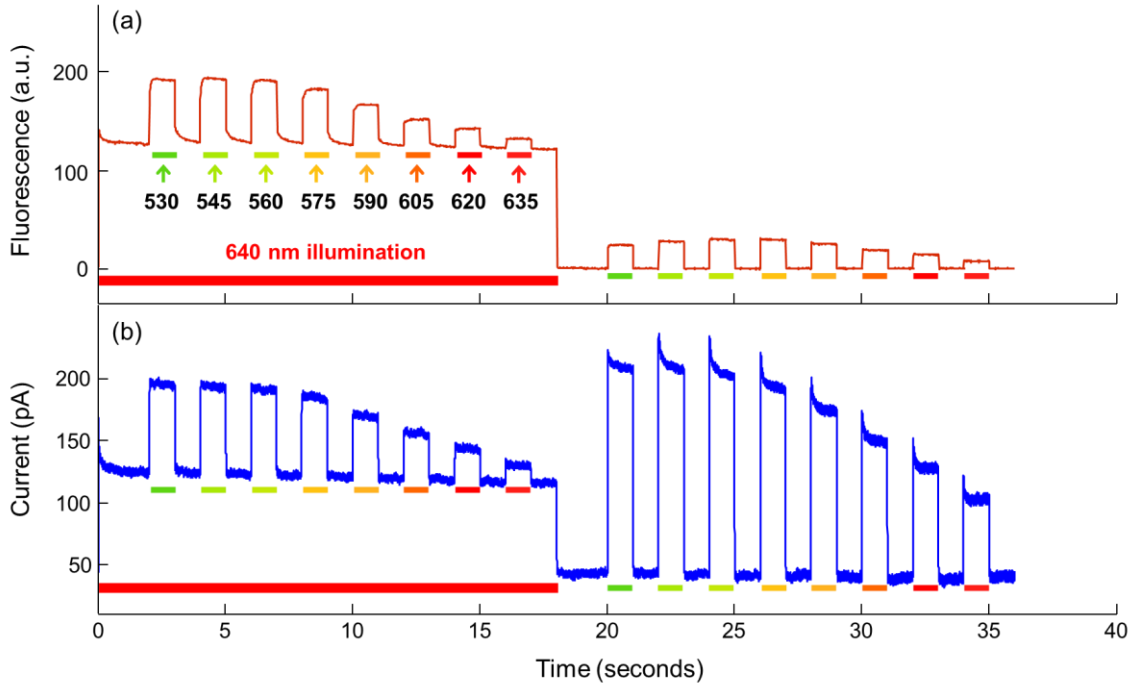

Figure S15. Effect of intense red illumination on fluorescence and photocurrent action spectra. A HEK cell expressing WT Arch was held at 0 mV under voltage clamp. (a) Fluorescence excitation spectrum and (b) photocurrent action spectrum of Arch under dim illumination (10 W/cm^2) in the presence (t = 0 to 18 s) or absence (t = 18 to 36 s) of intense red illumination (~1000 W/cm^2, 640 nm). Addition of intense red light caused slow (~200 ms) transients in fluorescence to appear, while causing the disappearance of slow (~300 ms) transients in photocurrent. Additionally, at wavelengths between 530 and 575 nm, addition of intense red light decreased the total photocurrent. This observation suggests a red light-dependent back-reaction or shortcut in the photocycle. The traces shown are an average of 3 cycles repeated on the same cell. The presence of slow dynamics in the fluorescence (640 nm on) in the absence of slow dynamics in the photocurrent; and slow dynamics in the photocurrent (640 nm off) in the absence of slow dynamics in the fluorescence, suggest that Arch contains transitions that are either spectrally or electrically silent. The presence of such transitions presents a severe challenge for efforts to elucidate the photocycle, and highlights the importance of multimodal spectroscopic and electrical measurements.

References:

1. Kralj JM, Douglass AD, Hochbaum DR, Maclaurin D, Cohen AE (2012) Optical recording of action potentials in mammalian neurons using a microbial rhodopsin. *Nat Methods* 9:90-95.

2. El-Sayed WSM, *et al.* (2002) Effects of light and low oxygen tension on pigment biosynthesis in halobacterium salinarum, revealed by a novel method to quantify both retinal and carotenoids. *Plant and Cell Physiology* 43:379-383.

3. Enami N, *et al.* (2006) Crystal structures of archaerhodopsin-1 and-2: Common structural motif in archaeal light-driven proton pumps. *J Mol Biol* 358:675-685.

4. Cartailler JP, Luecke H (2003) X-ray crystallographic analysis of lipid-protein interactions in the bacteriorhodopsin purple membrane*. *Annu Rev Biophys Biomol Struct* 32:285-310.